

GPO PRICE \$ \_\_\_\_\_

CFSTI PRICE(S) \$ \_\_\_\_\_

Technical Report 1

NASA-JPL (5926-9)

Hard copy (HC) \_\_\_\_\_

Contract No. 950875

Microfiche (MF) \_\_\_\_\_

# 653 July 65

Jet Propulsion Laboratory  
California Institute of Technology  
Pasadena, California

Failure of an Inert Composite Propellant  
under Multiaxial Stress Fields

by

M. G. Sharma and C. K. Lim

FACILITY FORM 602

N 65-35 109

(ACCESSION NUMBER)

(THRU)

(PAGES)

(CODE)

(NASA CR OR TMX OR AD NUMBER)

(CATEGORY)

The Pennsylvania State University  
Department of Engineering Mechanics  
University Park, Pennsylvania

March 1965

REF 3 2859

Technical Report 1

NASA-JPL (5926-9)

Contract No. 950875

*under NAS 7-100*

Jet Propulsion Laboratory  
California Institute of Technology  
Pasadena, California

Failure of an Inert Composite Propellant  
under Multiaxial Stress Fields

by

M. G. Sharma and C. K. Lim

The Pennsylvania State University  
Department of Engineering Mechanics  
University Park, Pennsylvania

March 1965

# Table of Contents

	<u>Page</u>
Preface . . . . .	11
I. Introduction . . . . .	1
II. Experimental Investigations . . . . .	3
(a) Material and specimen preparation . . . . .	3
(b) Mechanical behavior of the test material. . . . .	6
(c) Description of apparatus . . . . .	8
(d) Strain measurement . . . . .	9
(e) Experimental program . . . . .	10
(f) Description of biaxial fracture testing . . . . .	11
(g) Experimental results . . . . .	11
III. Theoretical Considerations. . . . .	11
(a) Octahedral shear stress criterion . . . . .	11
(b) Octahedral shear strain . . . . .	12
(c) Rivlin and Thomas failure criterion . . . . .	13
(d) Total strain energy at fracture under biaxial stress fields. . . . .	16
IV. Discussion of Results . . . . .	18
V. Conclusions. . . . .	19

## Preface

This report is the first of a series of technical reports on the research work conducted under research project entitled "A test program to determine the mechanical behavior of solid fuel propellants". The work reported here particularly refers to the evaluation of failure criteria of an inert composite propellant under five biaxial tension stress fields. The effect of rate of loading on failure behavior of the material is considered. The report describes a new biaxial testing machine used for failure studies of the inert composite propellant. Possibilities of describing failure in terms of octahedral shear stress, octahedral shear strain and maximum strain energy hypotheses are discussed.

Failure of an Inert Composite Propellant under  
Multiaxial Stress Fields

by

M. G. Sharma and C. K. Lim

I. Introduction

In recent years great effort has been directed towards the understanding of failure of composite elastomeric materials under various complex loading and environmental conditions. This has become important because solid fuel grains in some of the present day rockets are made of composite materials. A clear understanding of fracture properties of these materials is very necessary to ensure the structural integrity of the rocket system. Fracture behavior of elastomeric materials has been studied from three points of view. The first approach seeks to relate failure to molecular structure of the materials.<sup>[1-6]\*</sup> Although this method has led to the better understanding of the influence of various molecular variables on failure properties, the results are still qualitative in nature and therefore have limited significance for design purposes. The second approach attempts to determine the stress field<sup>[7-10]</sup> around an existing crack and from this information finds the conditions necessary for the crack to propagate and ultimately give rise to catastrophic failure. The above method has been used extensively to study fracture behavior of metallic materials. However, it presents mathematical difficulties when applied to composite materials that display large deformations resulting in non-linear response.

---

\* Numbers in brackets refer to Bibliography at the end.

In a somewhat similar treatment as the last method, which does not require the determination of the stress distribution in the vicinity of a crack, but requires only the strain energy of the system with a crack, Criteria of failure for rubber composite systems has been suggested in terms of a characteristic energy of tearing<sup>[11-14]</sup>. Even though this method provides a meaningful criterion of failure, still it falls short of the description of actual behavior due to the following reasons. The method does not take into account the effect of rate of loading on fracture. Secondly, it ignores what changes take place in the vicinity of a crack that is propagating. The third approach attempts to study the circumstances under which failure occurs. This is characterized by the existence of certain critical functions of stress or strain which when exceeded in a stressed material give rise to failure. This procedure has been found to be suitable for design purposes. Especially in the field of metallic materials, this method of describing failure has been used extensively<sup>[15-17]</sup>. But for non-metallic materials such as polymers, this procedure is being recently applied<sup>[18-22]</sup>. Application of this method requires the determination of a critical function (either of stress or of strain) experimentally. Investigations on various materials indicate that there is no universal criterion that is applicable to all materials. For each material, the critical function is to be determined from various multiaxial failure experiments. Stress states chosen for each of the multiaxial failure experiments must correspond to stress states in all the eight octants of the principal stress or principal strain space. Effect of temperature and the rate of loading introduce additional

complications in the evaluation of the critical functions. The effect of rate of loading has been studied by the authors for a limited number of multiaxial stress conditions. In order to clearly define the behavior of inert propellants for all complex loading and environmental histories, a program that includes failure tests for various multiaxial stress histories and temperatures is imperative. This report describes the first phase of the work in achieving the above objective. The multiaxial failure studies reported here pertain to the first quadrant of the principal stress space. The experimental data has been scrutinized closely to determine any critical function in terms of the principal stresses or principal strains, that define failure. Various functions such as a function representing octahedral shear stress or octahedral shear strain at fracture have been found for various multiaxial stress fields and two rates of loading. Assuming the material as neo-Hookean<sup>[23]</sup> (which has been shown to be approximately true), strain energies at fracture have been determined for various biaxial stress fields. Similarly, assuming the material as linear viscoelastic (which also can be shown to be approximately true), total strain energies at fracture have been determined for various stress fields using the tension creep compliance function, the bulk compliance function for the material and the Boltzmann superposition principle.

## II. Experimental Investigations

### (a) Material and specimen preparation.

The material used in this investigation is a composite dummy propellant that is a copolymer of Butadiene and Acrylic acid crosslinked with Epon 828. Finely divided aluminum of particle size 10 micron is used as a filler agent in the preparation of the material.

The proportion of various constituents in the dummy propellant is the following:

- |                                                   |       |
|---------------------------------------------------|-------|
| (1) Hycar 2000 x 131, B.F. Goodrich Chemical Co., | 24.4% |
| (2) Epon 828, Shell Development                   | 5.7%  |
| (3) H-10 Aluminum, Valley Aluminum                | 69.9% |

The procedure for the preparation of the dummy propellant as recommended by the Allegany Ballistics Laboratory, Cumberland, Maryland is described as follows.

The ingredients are added in a container in the order given above and treated for half an hour at 180°F. They are mixed thoroughly until the aluminum is completely dispersed. This operation must be done in a properly vented area. To decrease the viscosity the mixture is put into an oven for one-half hour at 180°F. The mixture is evacuated for approximately thirty minutes in a container large enough to allow for an expansion five times its original volume. After evacuation, the mixture is placed in the oven for an additional heating period of fifteen minutes (to decrease viscosity for casting operations). Next the mixture is poured into a preheated mold (180°F) and cured for three days at 180°F.

Preparation of void free specimens was a formidable problem. After considerable effort this was finally solved by preventing entrapping of any air through effective evacuation process. Plans are underway to improve the quality of specimens still further by casting the specimens with the mold maintained under high vacuum. In addition, the removal of the specimens from the mold without damaging them posed a serious problem. This was also solved by application of the proper amount of silicone grease

~~specimen~~ to the inner wall of the mold and the mandrel. Care was taken to remove the cast specimens without any prestressing. A typical tubular specimen used in this investigation is shown in Fig. 1 and a flat specimen used to study uniaxial tension properties is shown in Fig. 2.

It was found that the mechanical behavior of the test material depends on the post curing period<sup>\*</sup>. To explore this, tension tests on tubular specimens (Fig. 1) post cured for 4, 6, 9, 18, 33 and 47 days were performed and the results are given in Fig. 3. Fig. 3 does not show any perceptible trend in the variation of stress-strain curves with post curing period. However, plotting true stress against the number of days of post curing for various fixed extension ratios indicated that stress for a given extension ratio fluctuates about a mean value, the amplitude of the wave of variation decreasing with the decrease in number of days of post curing (see Fig. 4). It can be also seen from Fig. 4 that the fluctuation of mechanical properties is less at low extension ratios. Based upon the mean stress values for given extension ratios, a mean stress-extension ratio curve is determined which is shown in Fig. 3. From Fig. 4, it can be seen that a slight difference in post curing in the range of 25 to 40 days results in appreciable change in uniaxial tension behavior. This observation is particularly important while selecting specimens for biaxial testing, where it was not always possible to test specimens post cured for the same period. In other words, the scatter due to changes in post curing period in the stress-strain curve under identical conditions of uniaxial tension loading can be expected to be less at lower post curing period

---

\*The post curing period is defined here as the total time that elapsed between the time of the removal of the specimen from the mold and the time of testing. During this period the specimens were maintained at 75°F and 50% humidity environment.

than at higher period. With this understanding, scatter in stress-strain curves at low post curing period, namely 4 and 6 days was evaluated from uniaxial tension tests and is shown in Fig. 5. It is interesting to find that the mean stress-strain curve determined from Fig. 4 falls within the scatter band in Fig. 5. Based upon the variation of stress with post curing time in Fig. 4, it can be said the scatter might have been greater if the post curing period was around 30 days. This point will be verified in our future tests. The above study with regard to the specimen selection suggests the following.

In order to obtain consistent experimental data with respect to the mechanical behavior of the inert composite propellant, the specimens must be standardized. The standardization could be achieved by conforming to the recipe closely while preparing the specimens and post curing the specimens under constant temperature ( $75^{\circ}\text{F}$ ) and 50% humidity for a specified number of days (preferably 5 to 6 days). In addition, to insure void free specimens, the testing must be done in a vacuum.

(b) Mechanical behavior of the test material.

The effect of rate of loading on the uniaxial tension behavior is studied by subjecting tubular specimens to monotonically increasing load at constant loading rates and observing the extension in the axial direction. The results are shown in Fig. 6. In the same figure are noted the stress values at fracture corresponding to various rates of loading.

The behavior of the material in creep is studied by subjecting flat specimens (Fig. 2) to constant values of loads and observing elongation in the axial direction of the specimens. The creep data is presented in

the form of variation of creep compliance function  $D(t)^*$  with  $\log t$  (where  $t$  = time) in Fig. 7. As is seen from the figure the creep compliance function varies with stress  $\sigma_0$ , implying the material is slightly non-linear viscoelastic.

However, Fig. 7 shows that the compliance function does not vary with stress in a consistent fashion. Therefore, for computation purposes a mean compliance function is obtained. The mean creep compliance curve is found to obey the following relation.

$$D(t) = D_0 + D \left( 1 - e^{-\frac{t}{\tau}} \right) + \frac{t}{\eta} \quad (1)$$

where  $D_0$  = initial compliance,  $(3.6 \times 10^{-3} \text{ psi}^{-1})$

$D$  = retarded elasticity,  $(4.5 \times 10^{-4} \text{ psi}^{-1})$

$\tau$  = retardation time,  $(1.09 \text{ hrs.})$

$\eta$  = flow viscosity.  $6.67 \times 10^5 \text{ (psi-hrs.)}$

Equation (1) represents a four element Kelvin model (see Fig. 8).

The behavior of the material under isotropic compression (triaxial compression) is found to be viscoelastic. In Fig. 8 is plotted the bulk creep compliance function  $B(t)$  obtained from volumetric creep experiments<sup>[24]</sup> against  $\log t$ . It was found that the creep behavior corresponded to a three element model (see Fig. 9). The equation for bulk creep compliance function then becomes

$$B(t) = B_0 + B \left( 1 - e^{-\frac{t}{\lambda}} \right) \quad (2)$$

$B_0$  = initial bulk compliance,  $(21.8 \times 10^{-7} \text{ psi}^{-1})$

$B$  = bulk retarded elastic compliance,  $(5.28 \times 10^{-7} \text{ psi}^{-1})$

$\lambda$  = retardation time.  $(2.5 \text{ hrs.})$

---

\* **Note:** The creep compliance function is the ratio of strain  $\epsilon$  to stress  $\sigma_0$  in a creep test.

(c) Description of apparatus.

The biaxial apparatus used in the present study was developed by the author and was built at the machine shop of the department. The important feature of the apparatus is that the effect of rate of loading on fracture behavior of soft rubberlike materials can be simultaneously studied for different biaxial stress fields. The complete biaxial apparatus with other accessories is shown in Fig. 10. The biaxial apparatus as such consists of a lower head which is common for all biaxial stress field tests and a top head which is variable depending upon the biaxial stress field under consideration (see Fig. 11). The apparatus is equipped with two sets of heads. In each set there are five heads corresponding to five biaxial stress fields. The first set of heads produce biaxial stress fields corresponding to the first quadrant in the principal stress coordinate system. A complete assembly of this top head and the bottom head with the specimen is shown in Fig. 12. The manner of subjecting the specimens to biaxial tension-tension stress fields with the heads can be explained in the following way. Nitrogen gas from tanks fed through port "A" pressurizes the specimen along the inner wall. At the same time the gas flows through port "B" into chamber "C". The gas pressure acting on face "D" subjects the specimen to an axial load proportional to the area of the face D. The stress ratios developed by the five heads corresponding to the stress fields in the first quadrant are listed in Table 1. Similarly the remaining set of heads correspond to biaxial tension-compression quadrant (second quadrant in the principal stress coordinate system.)

A complete schematic of the biaxial apparatus with the various accessories is shown in Fig. 13. The specimen in a particular biaxial

fracture test is subjected to predetermined pressure histories (linear rate) by a closed loop feed back control system consisting of a data track function generator, a servac controller, a servovalve, a pressure transducer and a high pressure nitrogen gas supply (see Fig. 13). The system is capable of imposing linear pressure rates up to 200 psi/sec. The packings used on the upper head at two points have been found to offer resistance to motion, thus imposing a load in axial direction, the magnitude of which was important for the evaluation of axial load on the specimen. The loads due to friction were evaluated for the various biaxial tension-tension heads and are given in Table 2. These were estimated for any head by subjecting the biaxial arrangement (top and bottom head) to pressure by nitrogen gas and noting the value of pressure necessary for the upper head just to move. The same experiment was conducted on all heads.

(d) Strain measurement.

The deformation of tubular specimens in the multiaxial experiments was evaluated by measuring the axial elongation and the variations in internal and external diameters of the specimens during the test. The measurements were made through clip gages developed and constructed by the co-author. These clip gages are specially suited for the measurement of a soft rubberlike material (such as the test material) that displays large deformation. The clip gages used for measurements are made of spring steel 0.01 inch thick and  $9/32$  inches wide. The detailed drawing of all the three gages used for measurement of axial extension, internal diameter and external diameter is given in Fig. 14. Four active

SR-4 strain gages (A-7 120 ohms) bonded to each gage in Fig. 14 form the four arms of the wheatstone bridge. The clip gages which measure the internal and external diameters are provided with shoes at their tips, conforming to the curvature of the specimens on the inside and outside. It is believed that this arrangement provides better contact of the gage with the specimen and also reduces the restraint of the gage on the specimen. The internal and external clip gages are capable of measuring displacement up to 0.7 in. and the clip gage for axial extension which has original gage length of 0.5 in. can measure elongation up to 0.3 in. The clip gages together with 906C Honeywell recorder can read elongation correctly to 0.002 in.

(e) Experimental program

The fracture behavior of the inert composite propellant was studied for a uniaxial and five biaxial stress fields. The stress fields are represented in terms of stress ratios equal to  $\alpha$  equal to 0, 0.32, 0.82, 1.29, 1.68 and 2.29

$$\left( \text{where } \alpha = \frac{\sigma_{22}'}{\sigma_{11}} = \frac{\text{nominal principal stress in tangential direction}}{\text{nominal principal stress in axial direction}} \right)$$

The behavior under these uniaxial and biaxial fields were observed at two rates of loading namely,  $k = 0.01$  and  $10$  psi/sec (where  $k$  represents nominal stress rate in the maximum principal stress direction). Three tests were conducted under identical conditions for each of the stress fields mentioned above. This gave an idea of the amount of scatter in the data.

f. Description of biaxial fracture testing.

Tubular specimens were subjected to internal pressure and axial load that depended on the top head size. The rate of pressure was held constant during any test. The pressure rate was pre-determined to keep the nominal stress ratio constant in any test. The tests were continued up to fracture. For some biaxial tests the pressure reached a maximum and then decreased at fracture. However, for some others fracture occurred at the maximum stress. During any test maximum pressure, internal and external diameters and axial extensions were noted at fracture. From the maximum pressure nominal axial and tangential stresses were determined. Knowledge of extension ratios at fracture allowed one to determine the true axial and tangential stresses.

g. Experimental results.

In Table 3 are given the data obtained from five biaxial and one uniaxial stress field experiments.

Fig. 15 shows the failure data plotted with respect to nominal principal stress coordinate system and in Fig. 16 the same is plotted in terms of true principal stress coordinate system. A picture of fractured or cracked specimens under various stress fields is shown in Fig. 17 for two rates of loading.

III. Theoretical Considerations.

a. Octahedral shear stress criterion.

Biaxial fracture studies<sup>[22]</sup> made on the same material indicated that octahedral shear stress criterion checked well with experimental results. Therefore it was thought proper to verify the above criteria for the present fracture tests. The octahedral shear stress criterion states that

when the octahedral shear stress under multiaxial stress field reaches the value of octahedral shear stress in uniaxial tension fracture occurs. That is

$$(\sigma_{11} - \sigma_{22})^2 + (\sigma_{22} - \sigma_{33})^2 + (\sigma_{33} - \sigma_{11})^2 = 2 \sigma_f^2 \quad \text{-----}(3)$$

$\sigma_f$  = fracture stress in uniaxial tension.

In Fig. 18 is shown the variation of nominal octahedral shear stress at fracture with biaxial stress ratio  $\alpha$ . The nominal octahedral shear stress has been calculated by assuming  $\sigma'_{33} = 0$  or  $\sigma'_{33} = -p$  for the two prescribed rates of loading. It can be seen that the influence of radial stress actually has the effect of increasing the octahedral shear stress and thus bring its value nearer to the value of octahedral shear stress in tension. It can be seen from the same figure that  $\tau'_{oct}$  reaches a limiting value at large values of  $\alpha$ .

(b) Octahedral shear strain.

When the deformation of the material is large, the failure can be represented in terms of a critical function of strain. This critical function can be octahedral shear strain<sup>[15]</sup> which is given by the following equation.

$$\gamma_{oct} = \frac{2}{3} \left[ (\epsilon_{11} - \epsilon_{22})^2 + (\epsilon_{22} - \epsilon_{33})^2 + (\epsilon_{33} - \epsilon_{11})^2 \right]^{1/2} \quad (4)$$

Noting  $\epsilon_{11} = \left( \frac{\lambda_1^2 - 1}{2} \right)$ , etc. equation (4) can be rewritten as

$$\gamma_{oct} = \frac{1}{3} \left[ (\lambda_1^2 - \lambda_2^2)^2 + (\lambda_2^2 - \lambda_3^2)^2 + (\lambda_3^2 - \lambda_1^2)^2 \right] \quad (5)$$

Figure 19 shows the variation of octahedral shear strain at fracture for various biaxial stress fields.

(c) Rivlin and Thomas failure criterion.

Rivlin and Thomas [11] have suggested a criterion of tearing for rubberlike materials, which is an extension of the Griffith fracture hypothesis for brittle materials. According to this criterion catastrophic tearing occurs in a rubbery material when the critical tearing energy,  $T$  is related to the elastic strain energy as follows.

$$T = - \frac{1}{t} \left( \frac{\partial W}{\partial C} \right)_\ell \quad (6)$$

where  $t$  = thickness of specimen

$W$  = elastic energy

$C$  = length of a crack

$\left( \frac{\partial W}{\partial C} \right)_\ell$  = the change in elastic strain energy with the change in the length of the crack corresponding to constant overall length in tension test.

For a material undergoing large deformation, the change in elastic strain energy due to a small crack can be shown to be [11]

$$\Delta W = k' C^2 t W_0 \quad (7)$$

where  $W_0$  = elastic strain energy stored in the material due to deformation before the formation of crack.

$k'$  = a factor that depends on extension ratio.

From equation (7)

$$\left( \frac{\partial W}{\partial C} \right)_\ell = 2k' C t W_0 \quad (8)$$

$W_0$  can be determined from uniaxial tension experiment. By finite deformation theory<sup>[25]</sup> it can be shown the following relation is found to hold in uniaxial tension.

$$\sigma_{11}' = 2 \left( \lambda_1 - \frac{1}{\lambda_1^2} \right) \left( \frac{\partial W_0}{\partial I_1} + \frac{1}{\lambda_1} \frac{\partial W_0}{\partial I_2} \right) \quad (9)$$

where  $\sigma_{11}'$  = nominal stress in the direction of tension load

$\lambda_1$  = axial extension ratio

$I_1, I_2$  = strain invariants

The ratio  $\sigma_{11}' / 2 \left( \frac{1}{\lambda_1^2} - \lambda_1 \right)$  is shown plotted in Fig. 20 against  $\frac{1}{\lambda_1}$  for the two rates of loading. As is seen from the figures, the experimental data can be fitted to horizontal straight lines, to give the following values

$$\begin{aligned} \frac{\partial W_0}{\partial I_1} &= G \\ \frac{\partial W_0}{\partial I_2} &= 0 \end{aligned} \quad (10)$$

where  $G$  is a constant that depends upon rate of loading.

The values of the constant for the two rates of loading determined from Fig. 20 are the following.

<u>Rate of Loading</u>	<u>Constant</u>
k (psi/sec)	G (psi)
0.01	95
10.00	115

Figure 21 verifies the values in the above table, where  $\lambda_2$  has been evaluated based upon diameter measurements.

Equation (10) indicates that the strain energy function for the material can be represented by

$$W_o = G(I_1 - 3) \quad (11)$$

Substitution of  $W_o$  from equation (11) in equation (8) gives

$$\left( \frac{\partial W}{\partial C} \right)_\ell = 2 k' C + G(I_1 - 3) \quad (12)$$

Using equation (12) the expression for critical tearing energy (equation (4)) becomes

$$T = 2 k' C G(I_1 - 3) \quad (13)$$

In order to evaluate  $T$  from equation (11), the value of  $k'$  must be evaluated experimentally<sup>[11]</sup>.

In the absence of the value of  $k'$ , an estimate of critical tearing energy per unit length of crack is obtained as follows.

$$\left( \frac{T}{2k'C} \right) = W_f = G(I_1 - 3) \quad (14)$$

Previously the importance of the energy stored in the material in the evaluation of a critical tearing energy criteria for the material has been indicated. In the following, attempts are being made to develop a criterion of failure based upon the total strain energy at fracture. This energy has been calculated from creep behavior of the material in uniaxial tension and volumetric compression. The behavior of the material has been assumed as linear viscoelastic.

(d) Total strain energy at fracture under biaxial stress fields.

The three dimensional stress-strain relations for a linear visco-elastic material<sup>[2,6]</sup> can be shown to be

$$\begin{aligned}\epsilon_{11} &= \left[ D(t) \sigma_{11} - \left( \frac{D(t)}{2} - \frac{B(t)}{6} \right) (\sigma_{22} + \sigma_{33}) \right] \\ \epsilon_{22} &= \left[ D(t) \sigma_{22} - \left( \frac{D(t)}{2} - \frac{B(t)}{6} \right) (\sigma_{33} + \sigma_{11}) \right] \\ \epsilon_{33} &= \left[ D(t) \sigma_{33} - \left( \frac{D(t)}{2} - \frac{B(t)}{6} \right) (\sigma_{11} + \sigma_{22}) \right]\end{aligned}\quad (15)$$

where  $D(t)$  = creep compliance function in uniaxial tension

$B(t)$  = creep compliance function in volumetric compression

$\epsilon_{11}, \epsilon_{22}, \epsilon_{33}$  = principal strains

$\sigma_{11}, \sigma_{22}, \sigma_{33}$  = principal stresses

Using equations (15) and the Boltzmann superposition principle, it is possible to predict strains for any given stress history. They are

$$\begin{aligned}\epsilon_{11} &= \left[ \int_0^t D(t-t') \frac{d\sigma_{11}}{dt'} dt' - \int_0^t \left( \frac{D(t-t')}{2} - \frac{B(t-t')}{6} \right) \frac{d}{dt'} (\sigma_{22} + \sigma_{33}) dt' \right] \\ \epsilon_{22} &= \left[ \int_0^t D(t-t') \frac{d\sigma_{22}}{dt'} dt' - \int_0^t \left( \frac{D(t-t')}{2} - \frac{B(t-t')}{6} \right) \frac{d}{dt'} (\sigma_{33} + \sigma_{11}) dt' \right] \\ \epsilon_{33} &= \left[ \int_0^t D(t-t') \frac{d\sigma_{33}}{dt'} dt' - \int_0^t \left( \frac{D(t-t')}{2} - \frac{B(t-t')}{6} \right) \frac{d}{dt'} (\sigma_{22} + \sigma_{11}) dt' \right]\end{aligned}\quad (16)$$

where  $t$  = present time,  $t'$  = past time.

For biaxial loading corresponding to

$$\text{stress ratio } \frac{\sigma_{22}}{\sigma_{11}} = \alpha$$

$$\text{stress rate } \dot{\sigma}_{11} = kt'$$

equation (16) becomes

$$\begin{aligned} \epsilon_{11} &= \left[ \left(1 - \frac{\alpha}{2}\right) k \int_0^t D(t-t') dt' + \frac{\alpha k}{6} \int_0^t B(t-t') dt' \right] \\ \epsilon_{22} &= \left[ \left(\frac{2\alpha - 1}{2}\right) k \int_0^t D(t-t') dt' + \frac{k}{6} \int_0^t B(t-t') dt' \right] \\ \epsilon_{33} &= \left[ - (1 + \alpha) k \int_0^t \left( \frac{D(t-t')}{2} - \frac{B(t-t')}{6} \right) dt' \right] \end{aligned} \quad (17)$$

Using equations (17) the total energy at fracture becomes

$$W_f = \int_0^{(\epsilon_{11})_f} \sigma_{11} d\epsilon_{11} + \int_0^{(\epsilon_{22})_f} \sigma_{22} d\epsilon_{22} \quad (18)$$

Table 4 lists the total energy at fracture for various biaxial stress fields, evaluated from experimental results, from equation (14) and from equation (18). Figure 22 shows the variation of total strain energy with biaxial stress ratio. The strain energies are calculated based upon equation (14), equation (18) and experimental results.

#### IV. Discussion of results.

The plot of experimental data in nominal principal stress space and the true stress space indicates that failure curves drawn through the mean points cut the vertical axis at a stress value less than the fracture stress in uniaxial tension. If the material is isotropic, fracture stress for pure circumferential tension (corresponding to  $\frac{\sigma_{22}}{\sigma_{11}} = \infty$  that is vertical axis) must be the same as the fracture stress for pure axial tension (corresponding to  $\frac{\sigma_{22}}{\sigma_{11}} = 0$  that is horizontal axis). As this is not found true, it is quite likely that anisotropy may be introduced due to pull away of the filler from binder, when the stress ratios take on values either near zero or infinity. In other words, when the stress ratios correspond to zero or infinity, extension ratios at fracture are much higher than when the stress ratios have a value somewhere in between. Due to larger strain it is quite possible that the pull away of the binder from filler takes place for these stress states.

In Fig. 18, for the octahedral shear stress criterion to hold, the experimental points should be on a straight line with the intercept equal to octahedral shear stress in uniaxial tension for a particular rate of loading. However, this has been found approximately true at low rate of loading, 0.01 psi/sec and not satisfactory for high rate of loading 10 psi/sec. It is interesting to note that the assumption of a stress of magnitude  $p$  in the radial direction actually helps to bring the curve nearer to the horizontal line representing octahedral shear stress criterion.

Figure 19 shows the variation of octahedral shear strain with stress ratio  $\alpha$ . Octahedral shear strain criterion appears to be good at low stress ratios and high rate of loading, 10 psi/sec. For other cases it does not seem to be applicable.

Equation (13) indicates that characteristic tearing energy for the material depends on the energy stored in the material. Therefore, any theoretical method of evaluating the total strain energy at fracture is worth consideration. Figure 22 shows that beyond a stress ratio  $\alpha = 0.375$  the prediction based upon linear viscoelastic theory is very good for rate of loading 10 psi/sec. But the prediction based upon the finite deformation theory deviates considerably. For the stress ratio below  $\alpha = 0.375$ , the prediction based upon the finite deformation theory is good. The reason for the above behavior may be explained as follows. At stress ratios below  $\alpha = 0.375$  the strains are larger in the axial direction. Therefore, finite deformation theory describes the behavior. When the stress ratio is larger than  $\alpha = 0.375$ , strains are small and linear viscoelastic theory compares better with experimental results. The predictions based upon finite elastic theory and linear viscoelastic theory are equally good at low rates of loading 0.01 psi/sec.

#### V. Conslusions.

- (1) The biaxial apparatus described in this report provides an excellent facility to study failure behavior of solid fuel propellants under various biaxial stress fields and at various rates of loading.
- (2) Failure curves in the principal stress space (see Figs. 15 and 16) indicate there exists induced anisotropy in the material at fracture perhaps due to dewetting occurring in certain biaxial stress states.
- (3) Maximum strain energy at fracture for various biaxial stress fields evaluated from creep behavior in tensile and volumetric (bulk) deformation agrees well with experimentally determined energy at fracture for most biaxial stress fields. However, for low biaxial stress ratios predictions based on the finite deformation theory agrees better.

### Bibliography

- [1] F. Bueche  
The Tensile Strength of Elastomers According to Current Theories.  
Rubber Chemistry and Technology, Vol. 32, p. 1269 (1959).
- [2] G.R. Taylor and S.R. Darin,  
The Tensile Strength of Elastomers.  
Journal of Polymer Science, vol. 17, p. 511 (1955).
- [3] F. Bueche,  
Tensile Strength of Rubbers,  
Journal of Polymer Science, vol. 24, p. 189 (1957).
- [4] A.M. Bueche,  
Ultimate Properties of Simple Elastomers,  
Journal of Polymer Science, vol. 19, p. 275 (1956).
- [5] F. Bueche,  
Tensile Strength of Plastics Above the Glass Temperature.  
Journal of Applied Physics, vol. 26, p. 1133 (1955).
- [6] F. Bueche and T. J. Dudek,  
Tensile Strength of Gum and Reinforced EPR and SBR Vulcanizates,  
Rubber Chemistry and Technology, vol. 37, p. 818 (1964).
- [7] J.W. Craggs,  
Fracture Criteria for Use in Continuum Mechanics,  
Fracture of Solids edited by D.C. Drucker, p. 51 (1962).
- [8] G.R. Irwin,  
Fracture Mechanics  
A Symposium in Naval Structural Mechanics, p. 557 (1960).
- [9] J.W. Craggs,  
On the Propagation of a Crack in an Elastic Brittle Material,  
Journal of Mechanics and Physics of Solids, vol. 8, p. 66.
- [10] G.I. Barenblatt,  
The Formation of Equilibrium Cracks during Brittle Fracture.  
General Ideas and Hypotheses. Axially Symmetric Cracks.  
PMM Journal of Applied Mathematics and Mechanics. Trans. Soviet  
Journal, vol. 23, p. 622 (1959).
- [11] R.S. Rivlin and A.G. Thomas,  
Rupture of Rubber I- Characteristic Energy for Tearing.  
Journal of Polymer Science, vol. 10, p. 291 (1953).
- [12] A.G. Thomas,  
Rupture of Rubber II. The Strain Concentration at an Incision.  
Journal of Polymer Science, vol. 18, p. 177 (1955).

- [13] H.W. Greensmith and A.G. Thomas,  
Rupture of Rubber III. Determination of Tear Properties.  
Journal of Polymer Science, vol. 18, p. 189 (1955).
- [14] M. L. Williams,  
The Fracture of Viscoelastic Materials.  
Fracture of Solids edited by D.C. Drucker, p. 157 (1962).
- [15] A. Nadai,  
Theory of Flow and Fracture of Solids,  
p. 175, McGraw-Hill (1950).
- [16] J.C. Jaeger,  
Elasticity, Fracture and Flow.  
Methuen (1956).
- [17] J. Marin,  
Engineering Materials, Their Mechanical Properties and Applications,  
Prentice-Hall, Inc. (1956).
- [18] M.L. Williams, P.J. Blatz and R.A. Schapery,  
Fundamental Studies Relating to System Analysis of Solid Propellants,  
Final Report Galcit 101 (SM 61-5).
- [19] Bulletin of the 3rd Meeting of the Interagency Chemical Rocket  
Propulsion Group.  
CPIA Publication No. 61V, Oct. 1964.
- [20] M.G. Sharma and C.K. Lin,  
Mechanical Properties of Solid Propellants for Combined States  
of Stress at Various Temperatures.  
Final Report to Allegany Ballistics Laboratory, Cumberland,  
Maryland, under Subcontract 70 NORD 16640.
- [21] M.G. Sharma and C.K. Lin,  
Experimental Investigations on Fracture of Polymers.  
A paper presented at the Regional Technical Conference of the  
SPE, Washington, D.C., June 4, 1964. To be published in the  
Transactions of the SPE.
- [22] M.G. Sharma,  
Failure of Polymeric Materials under Biaxial Stress Fields,  
A paper presented at the Regional Technical Conference of the  
SPE in Newark, N.J., November 1964. To be published in the  
Transactions of the SPE.
- [23] R.S. Rivlin,  
Large Elastic Deformations of Isotropic Materials I. Fundamental  
Concepts.  
Phil. Trans. R. Soc., vol (A) 240, pp. 459-490 (1948).

- [24] M.G. Sharma and V.D. McCarty,  
Experimental Investigations on the Dynamic Compressibilities of  
Polymeric Materials.  
A paper presented at the Fifth International Symposium on High  
Speed Testing in Boston, Mass., March 1965.
  
- [25] L.R. Treloar,  
Physics of Rubber Elasticity,  
Oxford, 1953.
  
- [26] A.J. Staverman and F. Schwarzl,  
Linear Deformation Behavior of Polymers,  
Chapter I in Die Physik der Hochpolymeren,  
Ed., Stuart, H.A., Springer-Verlag, 1956.

Table 1. Biaxial Stress Ratios for Various Cylindrical Heads  
of the Biaxial Testing Machine

No.	Diameter of Cylinder Head $D_c$ (in)	Biaxial Stress Ratio $\alpha$
1	1.5	2.289
2	1.75	1.682
3	2.00	1.288
4	2.50	0.824
5	4.00	0.322

Table 2. Friction Force in Cylindrical Head Assembly  
of the Biaxial Testing Machine

Diameter of Cylinder Head $D_c$ (in)	Friction Force $f$ (lb)
1.5	5.01
1.75	4.23
2	3.54
2.5	2.7
4.00	3.09

Table 3. Fracture Data for Various Biaxial Stress Fields

No. of Test	Biaxial Stress Rate	Rate of Loading	Maximum Pressure	Pressure at Fracture	Nominal $\sigma_{11}$	Fracture Stress $\sigma_{22}$	Extension Ratio At Fracture			True Stress At Fracture	
							$\lambda_1$	$\lambda_2$	$\lambda_3$	$\sigma_{11}$	$\sigma_{22}$
1	2.288	0.01	25	25	27.5662	71.1538	0.99800	1.16351	0.84808	27.9366	102.2676
2	2.288	0.01	18	18	18.8626	51.2307	1.0000	1.12184	0.89615	18.7624	66.3991
3	2.288	0.01	24.6	24.6	2.70688	70.0153	0.99800	1.15517	0.85385	27.4438	99.0649
4	2.288	0.01	17	17	17.6193	48.3846	0.99600	1.10747	0.88077	18.0631	63.0262
1	1.681	0.01	20.6	20.6	32.0483	58.6306	1.0200	1.10172	0.88077	33.0270	75.9231
2	1.681	0.01	23.2	23.2	36.4484	66.0306	1.0430	1.17385	0.80962	38.3519	100.9558
3	1.681	0.01	25.6	25.6	40.5100	72.8614	1.0270	1.16810	0.81731	42.4322	109.6282
1	1.287	0.01	22.1	22.1	46.3879	62.8999	1.0400	1.10805	0.86154	48.5929	84.0589
2	1.287	0.01	21.4	21.4	44.8407	60.9076	1.0520	1.13190	0.82115	48.2437	88.0056
3	1.287	0.01	24.9	24.9	52.5772	70.8691	1.0480	1.14741	0.83269	55.0291	102.3603
1	0.824	0.01	19.00	19.00	63.7225	54.0769	1.1040	1.08190	0.83654	70.4079	72.7241
2	0.824	0.01	20.3	20.3	68.2125	57.7769	1.1130	1.08592	0.83269	75.4365	78.4340
3	0.824	0.01	20.8	20.8	69.9394	59.1999	1.1140	1.09540	0.83077	76.8542	81.3704
4	0.824	0.01	22.5	22.5	75.8108	64.0384	1.1310	1.11236	0.78654	86.6493	95.2262
1	0.322	0.01	12.2	12.2	107.1655	34.7230	1.2460	0.9595	0.8442	132.2991	40.2961
2	0.322	0.01	11.2	11.2	98.3238	31.8769	1.1820	0.9672	0.8885	114.4156	35.200
3	0.322	0.01	10.0	10.0	87.7137	28.4615	1.1800	0.9675	0.8942	101.3804	31.204

Table 3. Fracture Data for Various Biaxial Stress Fields (continued)

No. of Test	Biaxial Stress Rate	Rate of Loading	Maximum Pressure	Pressure at Fracture	Nominal Stress		Extension Ratio At Fracture			True Stress At Fracture	
					$\sigma_{11}'$	$\sigma_{22}'$	$\lambda_1$	$\lambda_2$	$\lambda_3$	$\sigma_{11}$	$\sigma_{22}$
1	0	0.01	8.8	8.8	77.1036	0	1.1440	0.9279	0.9519	87.2940	0
2	0	0.01	11.2	11.2	98.3238	0	1.1440	0.9049	0.9173	118.4541	0
3	0	0.01	8.6	8.6	75.3353	0	1.1380	0.9376	0.9519	84.4032	0
4	0	0.01	8.8	8.8	77.1036	0	1.1240	0.9026	0.90962	93.9136	0
1	2.288	10	38	38	43.730	108.154	1.010	1.1675	0.8327	44.9808	159.2841
2	2.288	10	44.4	44.4	51.687	126.369	1.0760	1.3833	0.8500	43.9582	219.5891
3	2.288	10	40.0	40.0	46.217	113.846	1.016	1.2287	0.8000	47.0166	185.5769
1	1.681	10	38.5	38.5	62.342	109.576	1.056	1.2402	0.8462	59.4054	169.575
2	1.681	10	42.6	42.6	69.280	121.246	1.104	1.3342	0.8289	62.6493	208.1568
3	1.681	10	41.3	40.4	65.557	114.984	1.098	1.3388	0.9019	54.2921	180.4648
1	1.287	10	41.4	40.4	86.8389	114.9845	1.1580	1.3414	0.8539	75.8199	192.1730
2	1.287	10	39.7	38.9	83.5232	110.7152	1.1680	1.3724	1.0077	60.3940	157.8271
1	0.824	10	42.0	42.0	143.1599	119.5383	1.2420	1.2690	0.6846	164.7878	239.4944
2	0.824	10	32.5	32.5	110.3488	92.4999	1.1480	1.1356	0.7846	123.8435	141.1520
3	0.824	10	37.2	35.6	121.0556	101.3229	1.2580	1.3411	0.7981	113.1050	182.3749
4	0.824	10	35.8	35.8	121.7464	101.8922	1.2200	1.2382	0.7096	138.5593	191.1274
1	0.322	10	21.2	21.2	186.7411	60.3384	1.3820	0.9703	0.7952	242.0362	75.9560
2	0.322	10	20.8	20.8	183.2044	59.1999	1.4260	0.9855	0.9067	205.0246	65.2454
3	0.322	10	19.5	19.5	171.7102	55.4999	1.4080	0.9862	0.8115	214.5453	69.5438
4	0.322	10	20.1	20.1	177.0152	57.2076	1.3940	0.9706	0.8279	220.3052	68.7976
1	0	10	23.8	23.8	209.7296	0	1.4400	0.8466	0.8423	294.1275	0
2	0	10	24.4	24.4	215.0347	0	1.3820	0.8494	0.8615	293.8385	0

Table 4. Total Strain Energy at Fracture For  
The Inert Composite Propellant

Rate of Loading k (psi/sec)	Biaxial Stress Ratio $\alpha$	Total Strain Energy at Fracture $W_f$ (psi)		
		Experimental	By Finite Deformation Theory	By Linear Visco- elastic Theory
0.01	0.000	7.3828	4.7	11.6394
0.01	0.000	4.9333	5.0	11.1013
0.01	0.000	9.0002	5.8	19.0948
0.01	0.000	6.2998	5.4	11.6394
0.01	0.824	8.4223	14.1	9.7690
0.01	0.824	5.6446	10.7	8.3033
0.01	0.824	5.6814	9.7	7.8957
0.01	0.824	5.1561	8.6	6.8823
0.01	1.29	10.9035	10.1	7.9220
0.01	2.29	5.0954	7.9	7.1424
0.01	2.29	5.0265	8.7	7.3959
10.0	0.000	44.3534	41.4	83.23
10.0	0.000	45.7472	53.7	79.21
10.0	0.824	20.1567	53.3	23.01
10.0	0.824	18.0138	85.0	22.77
10.0	0.824	12.9020	22.7	18.97
10.0	0.824	38.5756	64.4	31.80
10.0	1.29	16.1245	73.9	17.97
10.0	1.29	14.8981	64.3	19.41
10.0	1.68	15.3515	53.4	17.97
10.0	1.68	26.7603	53.3	18.77
10.0	1.68	13.3778	27.4	16.31
10.0	2.29	19.5043	60.9	21.77
10.0	2.29	8.0023	11.9	15.96
10.0	2.29	11.1639	21.3	17.65

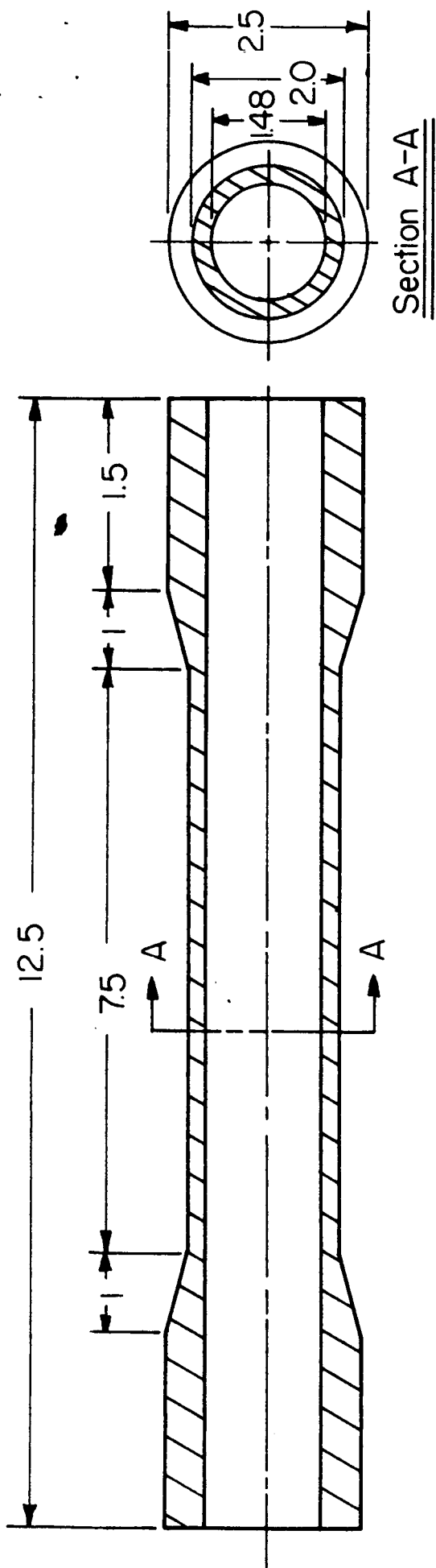


FIG.1 A TYPICAL TUBULAR SPECIMEN

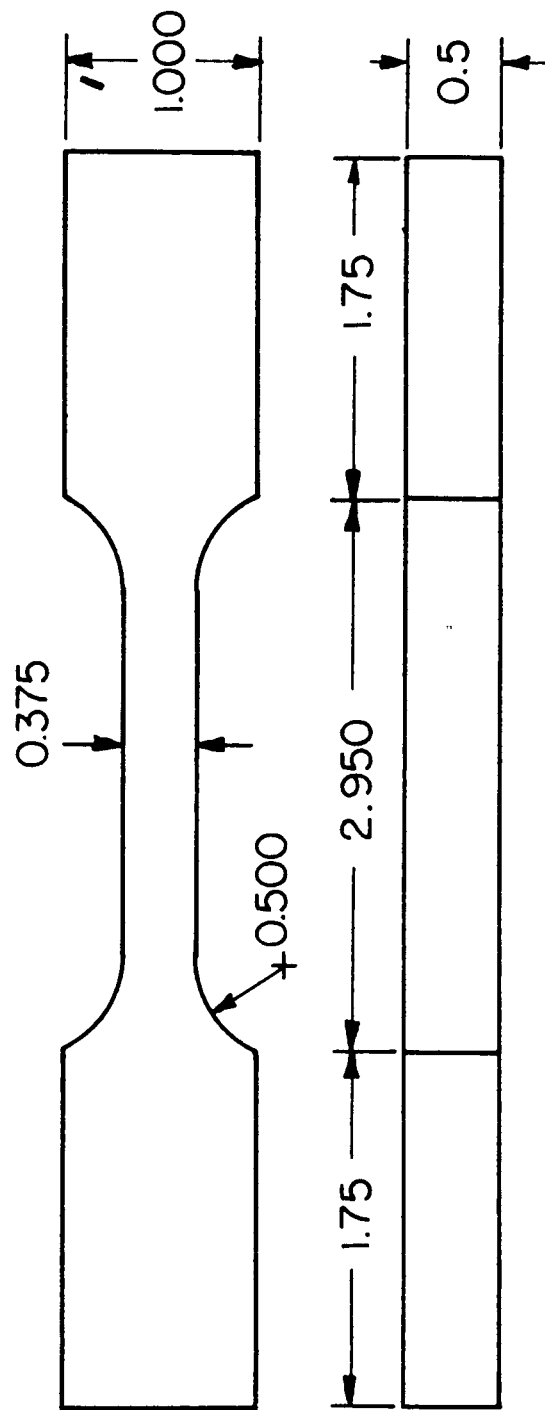


FIG.2 A TYPICAL FLAT SPECIMEN (JANAF)

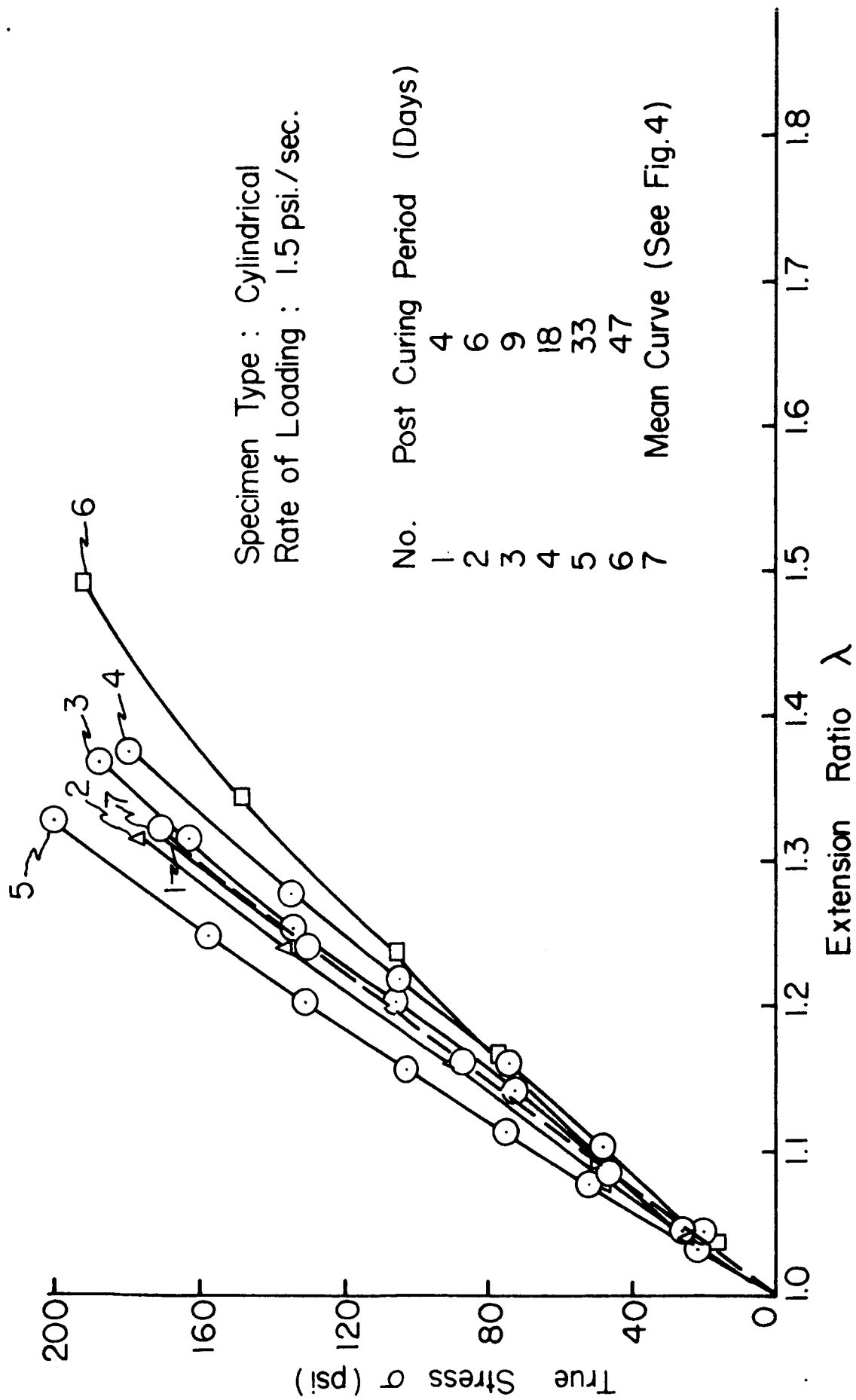


FIG. 3 EFFECT OF POST CURING PERIOD ON THE MECHANICAL BEHAVIOR OF INERT PROPELLENT IN UNIAXIAL TENSION

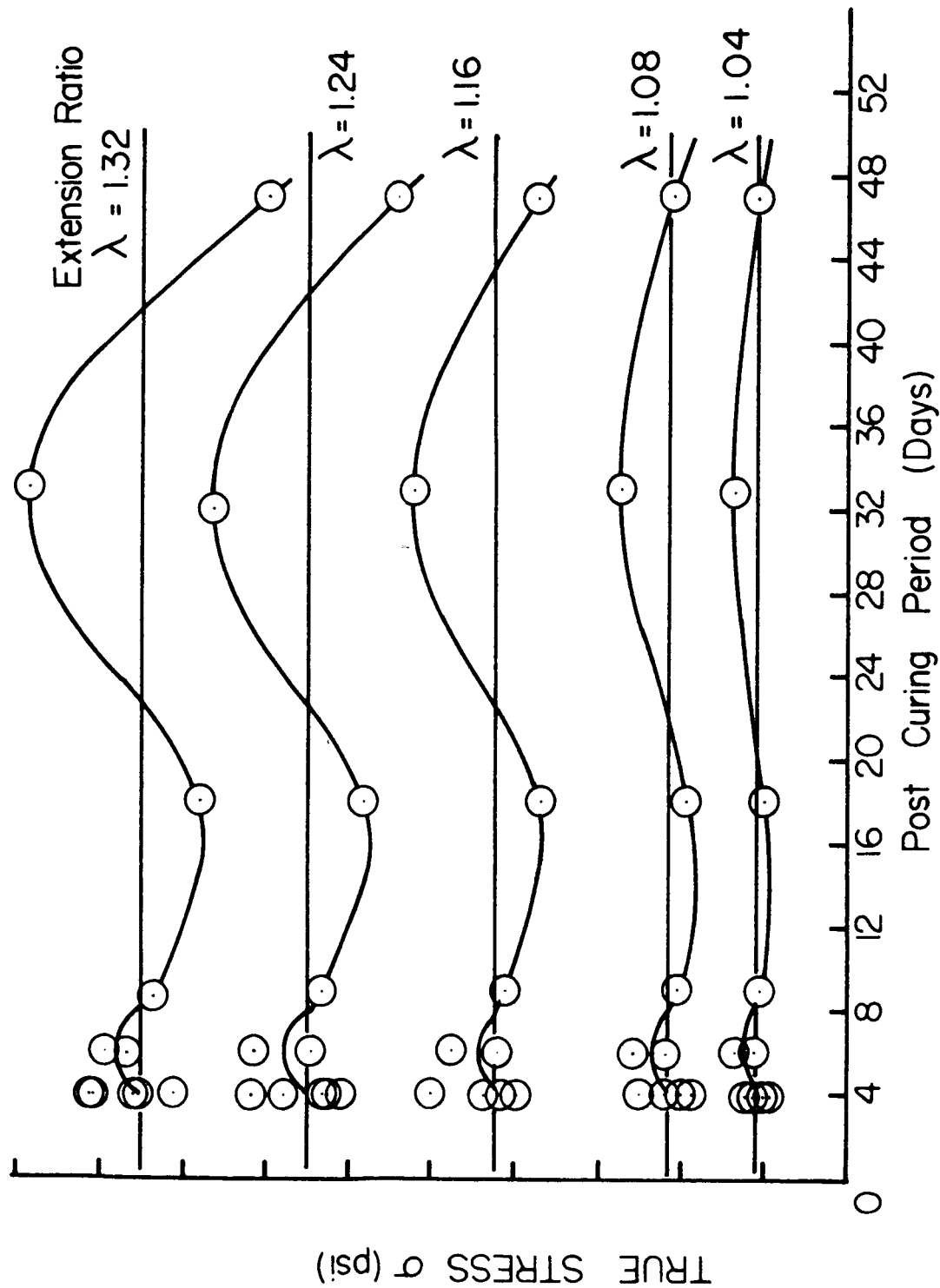


FIG. 4 VARIATION OF TRUE STRESS WITH THE DAYS OF POST CURING  
FOR 'INERT' COMPOSITE PROPELLANT

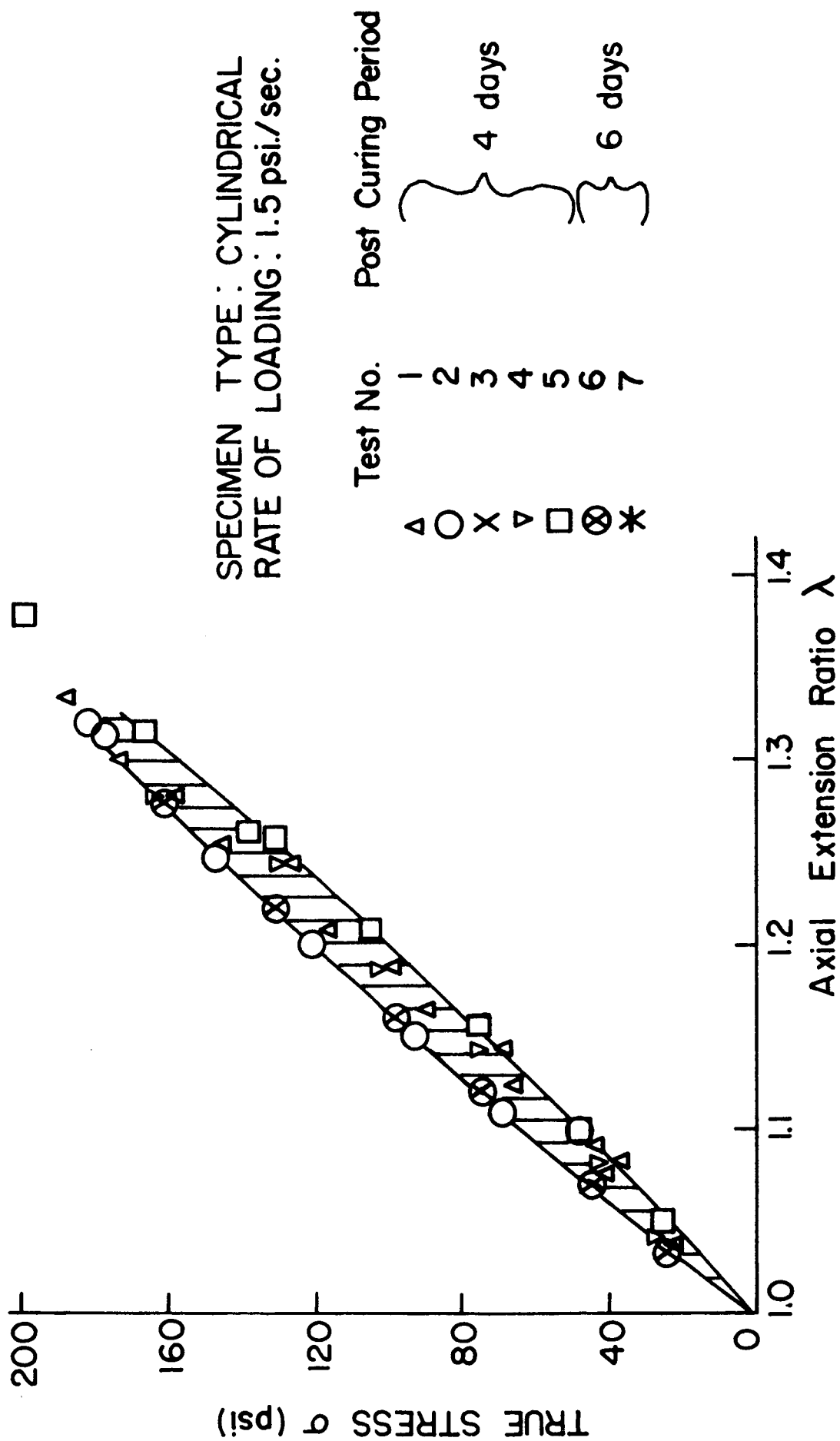


FIG. 5 TRUE STRESS vs. AXIAL EXTENSION RATIO CURVE FOR THE  
INERT COMPOSITE PROPELLANT

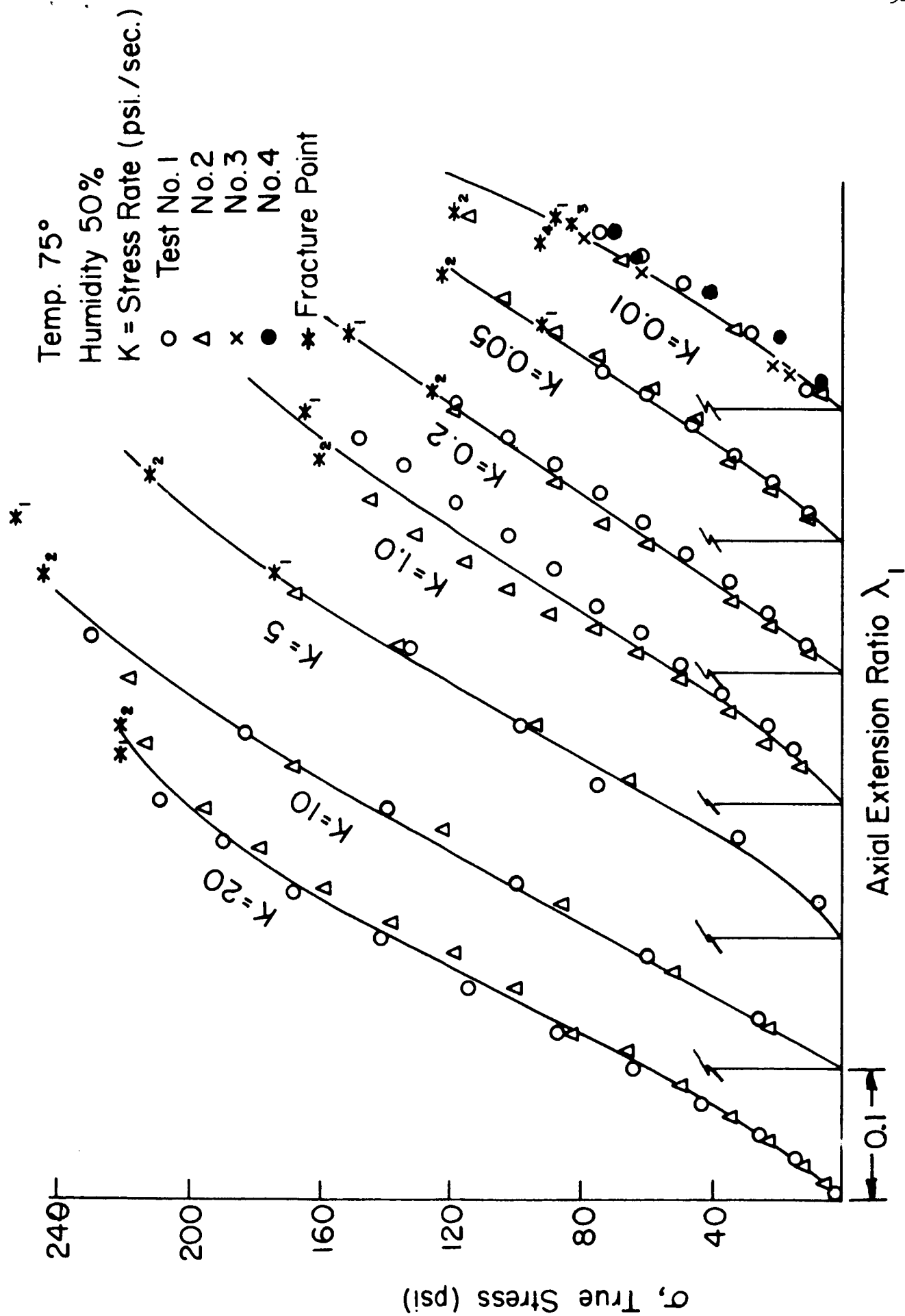


FIG. 6 TRUE STRESS vs AXIAL EXTENSION RATIO FOR THE INERT COMPOSITE PROPELLANT

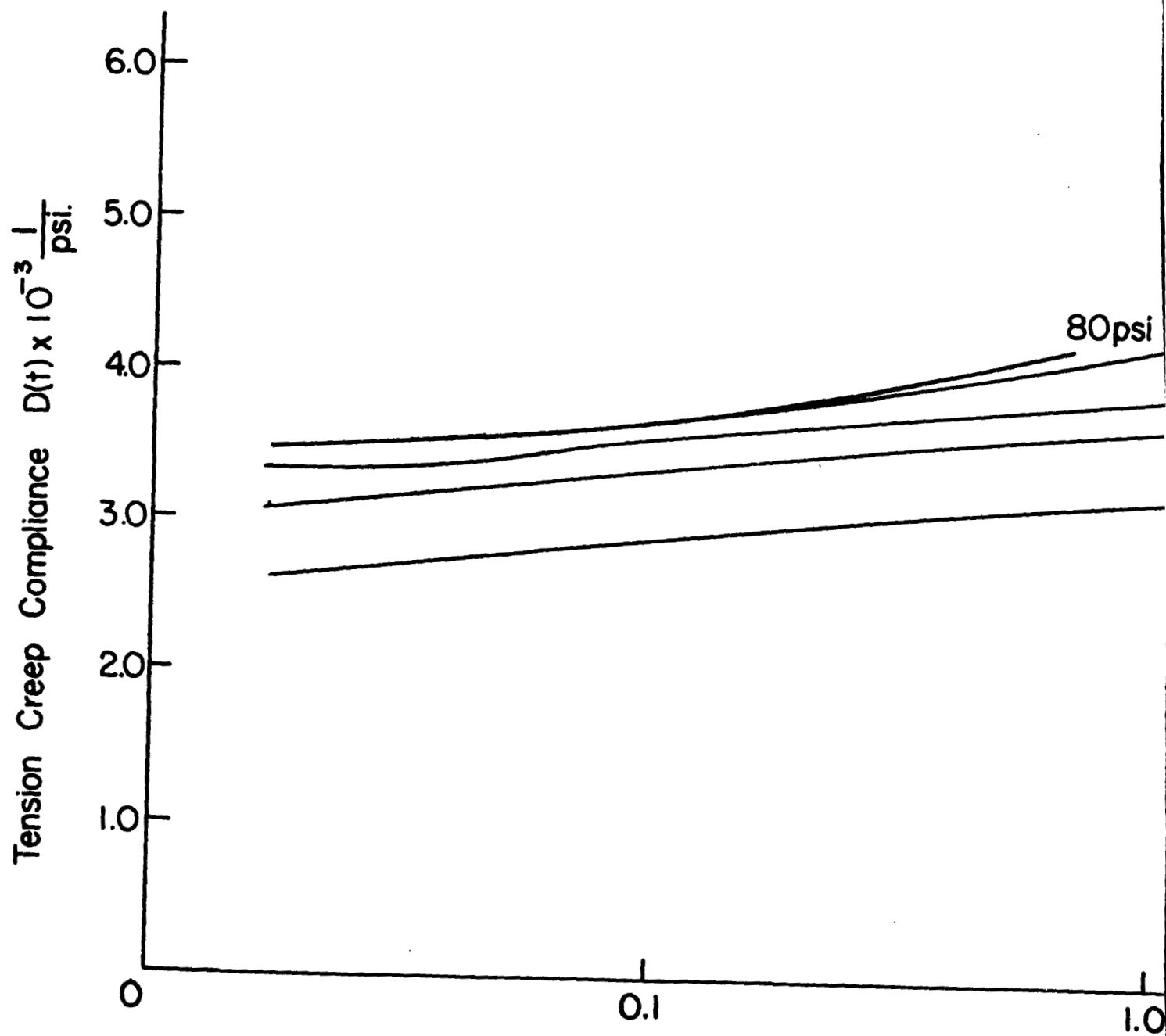
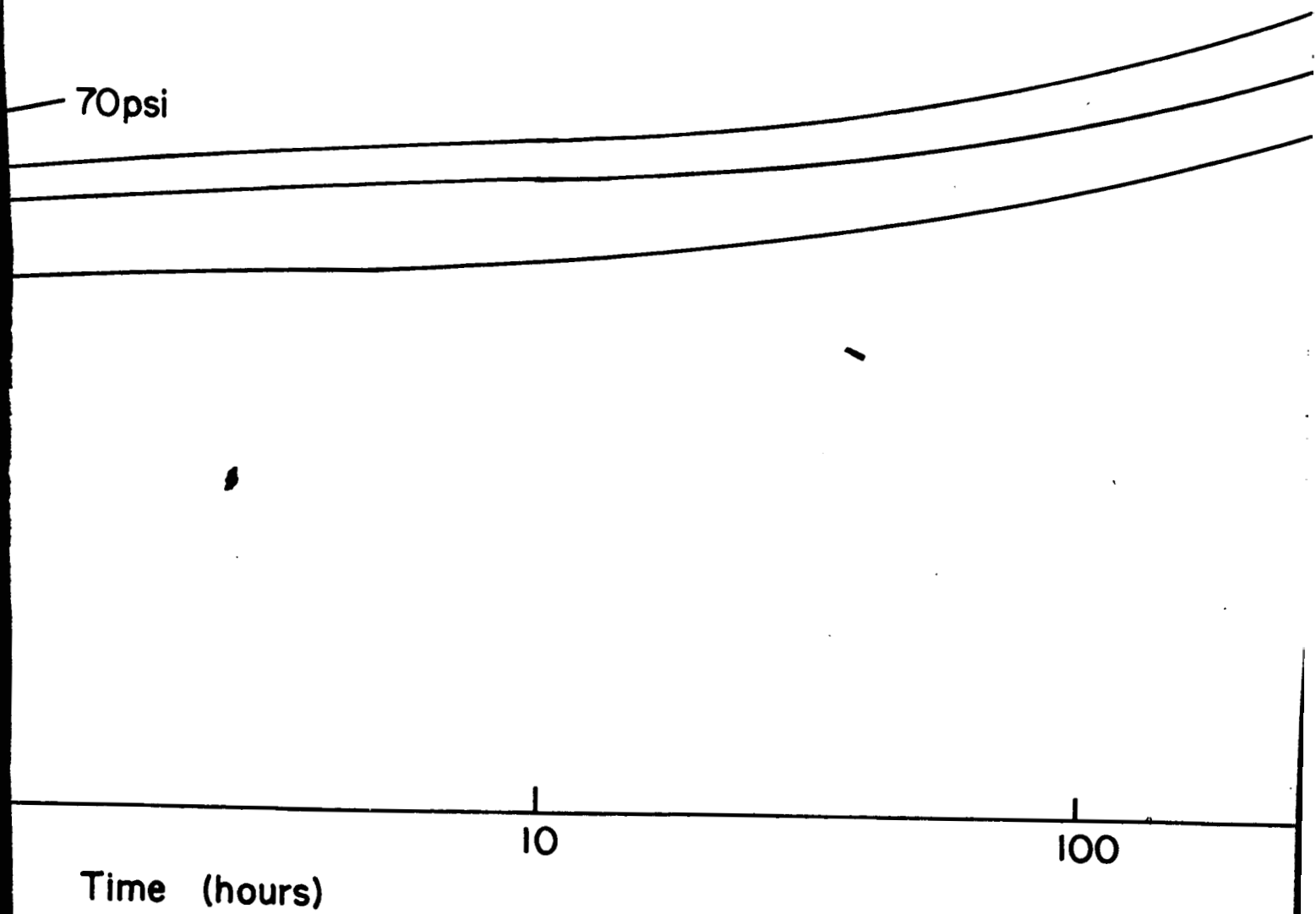
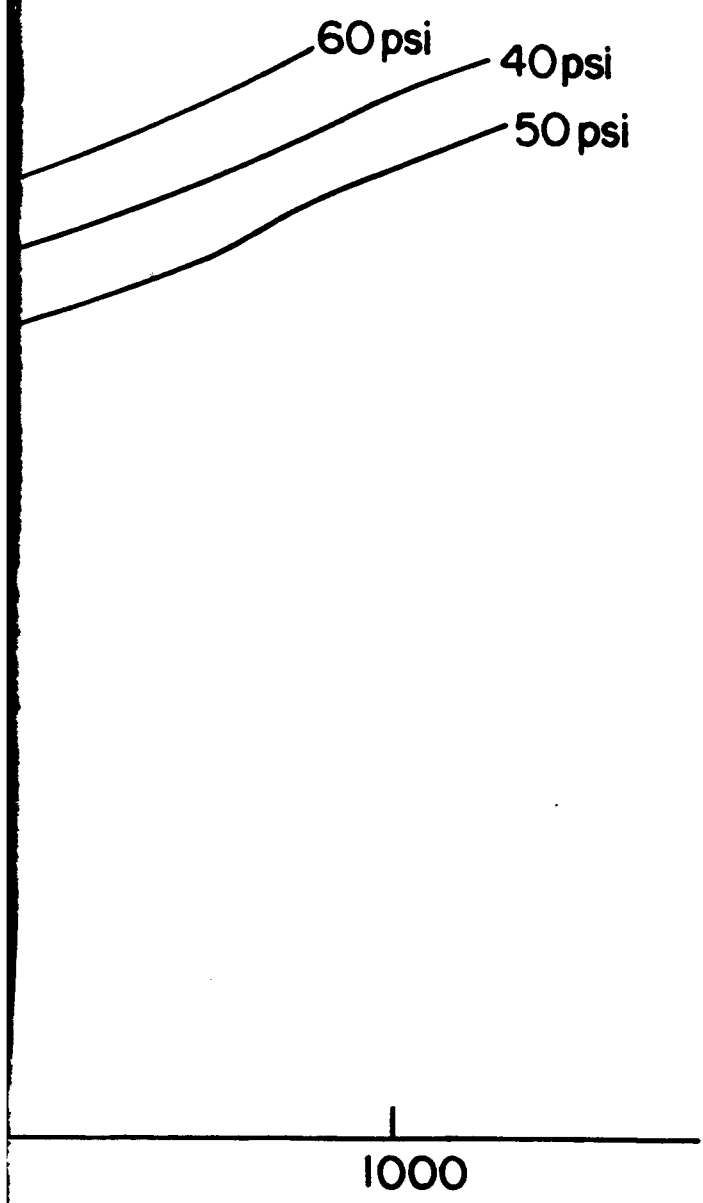


FIG. 7 VARIATION OF TENSION CREEP



COMPLIANCE WITH TIME FOR THE INERT COMPOSITE PROPELL



ANT

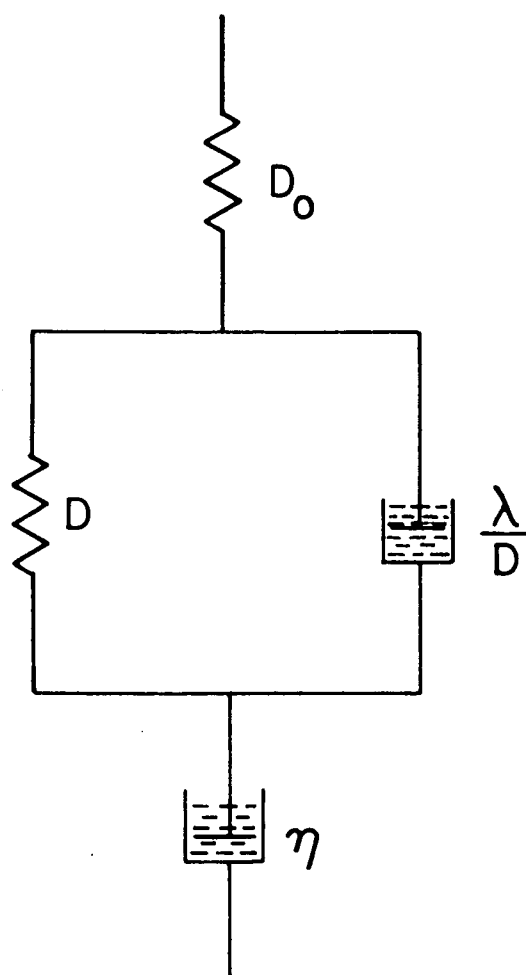


FIG. 8 A FOUR ELEMENT KELVIN  
MODEL FOR TENSION CREEP

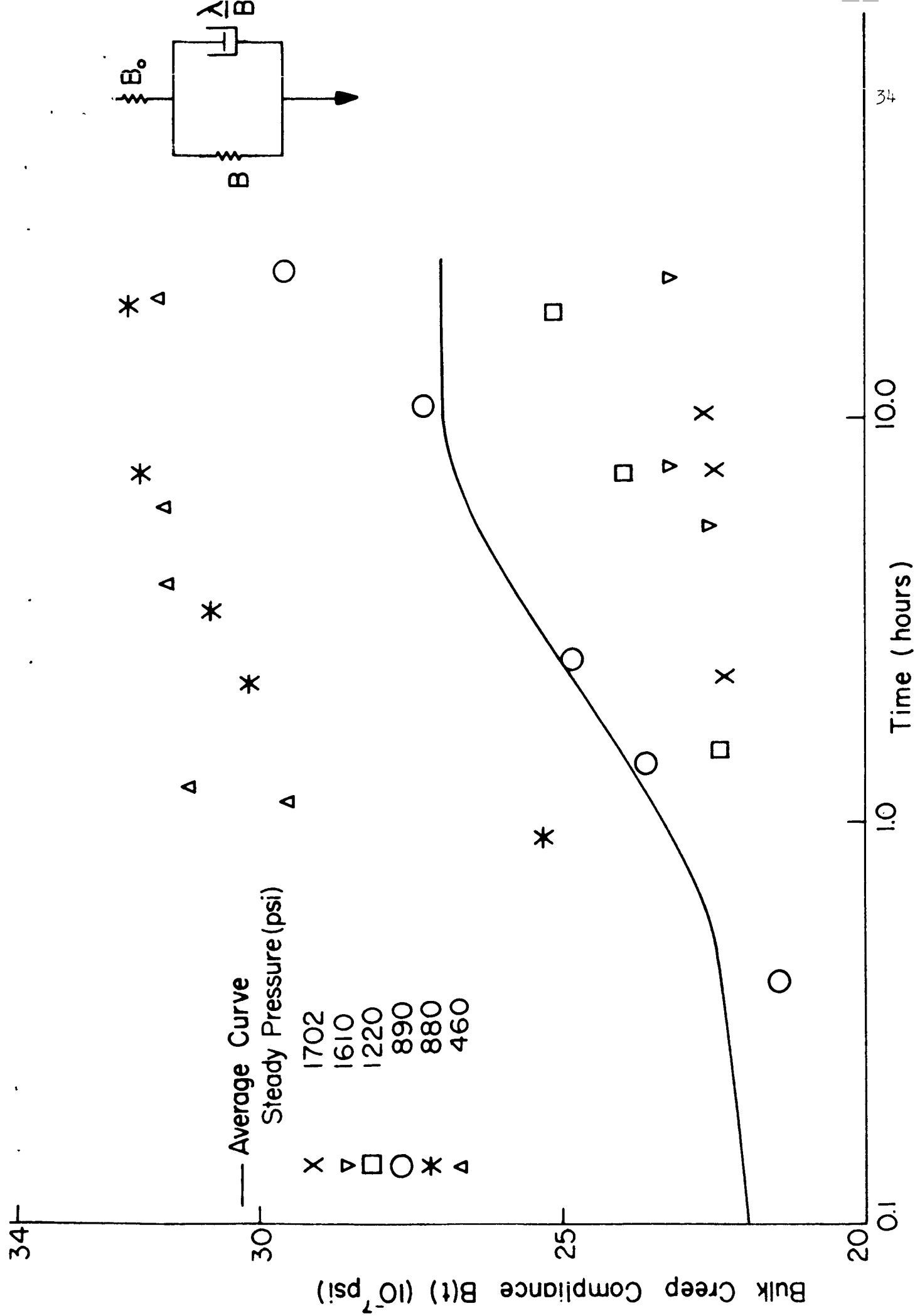


FIG. 9 VARIATION OF BULK CREEP COMPLIANCE WITH TIME FOR THE INERT COMPOSITE PROPELLANT



Fig. 10 Experimental Arrangement for Multi-axial Fracture Studies

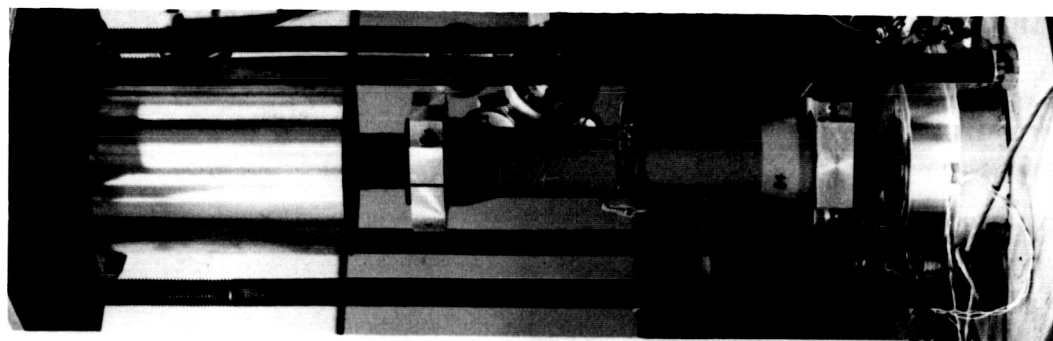


Fig. 11 Close Up View of Specimen Head Assembly

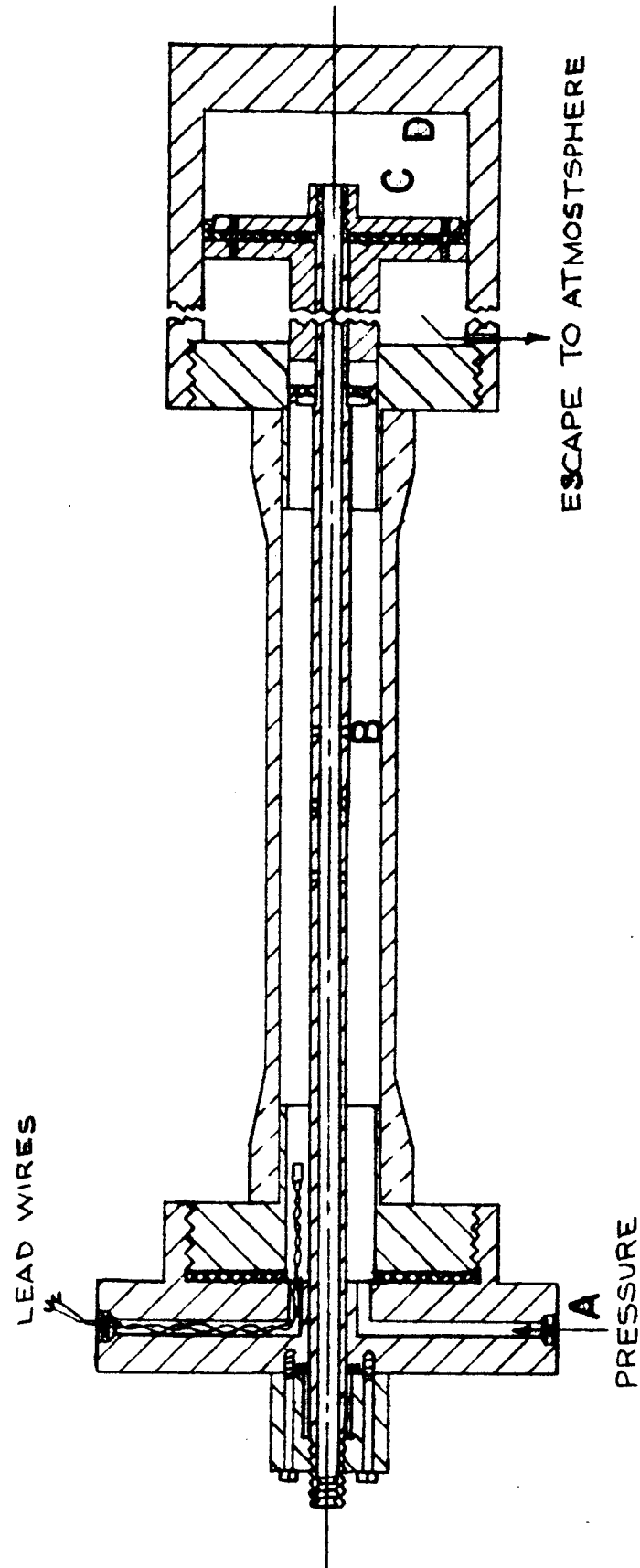


FIG. 12 SPECIMEN HEAD ASSEMBLY OF THE BIAXIAL APPARATUS

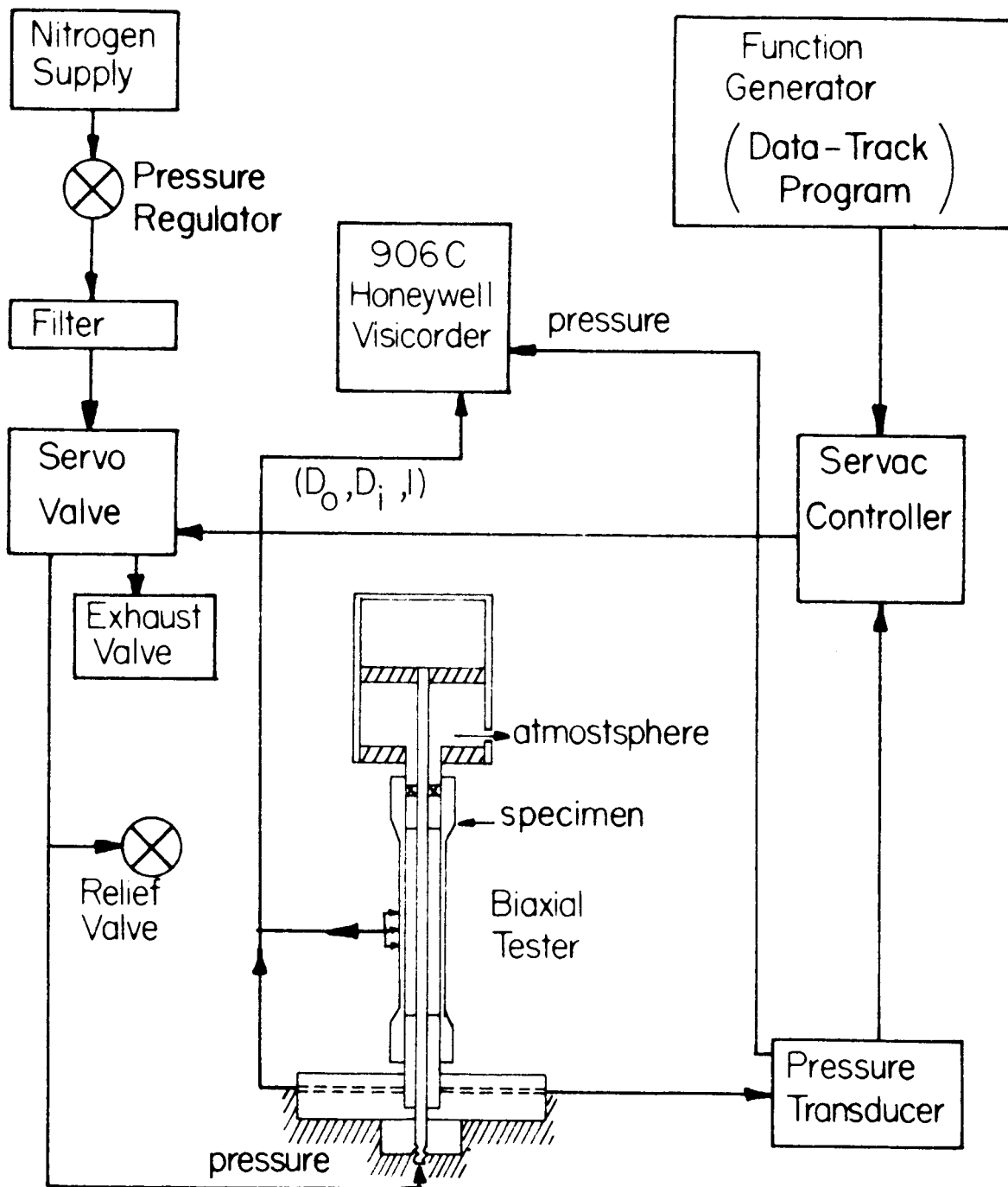
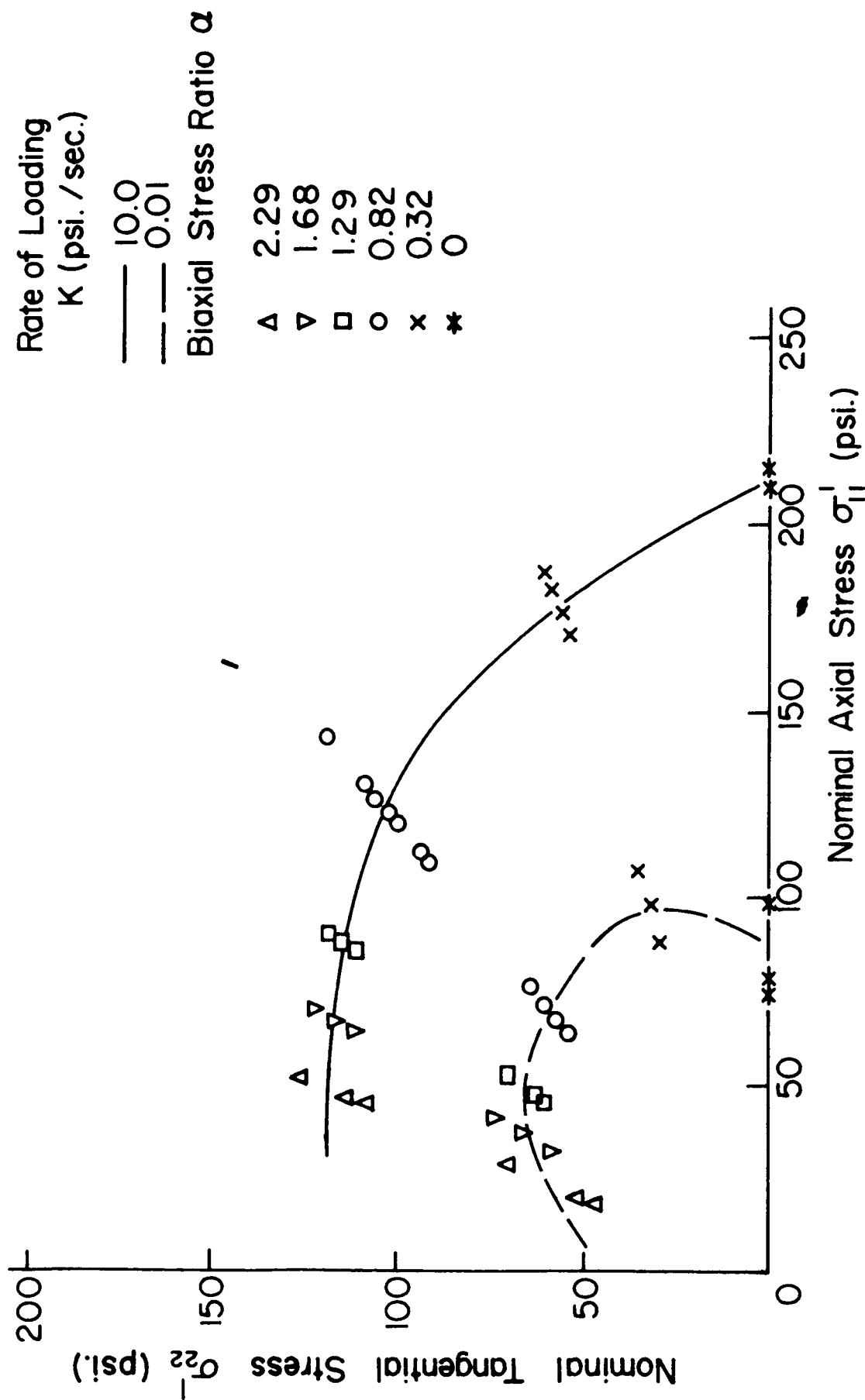


FIG. 13 SCHEMATIC OF MULTIAXIAL LOADING SYSTEM



FIG. 14 CLIP GAUGES



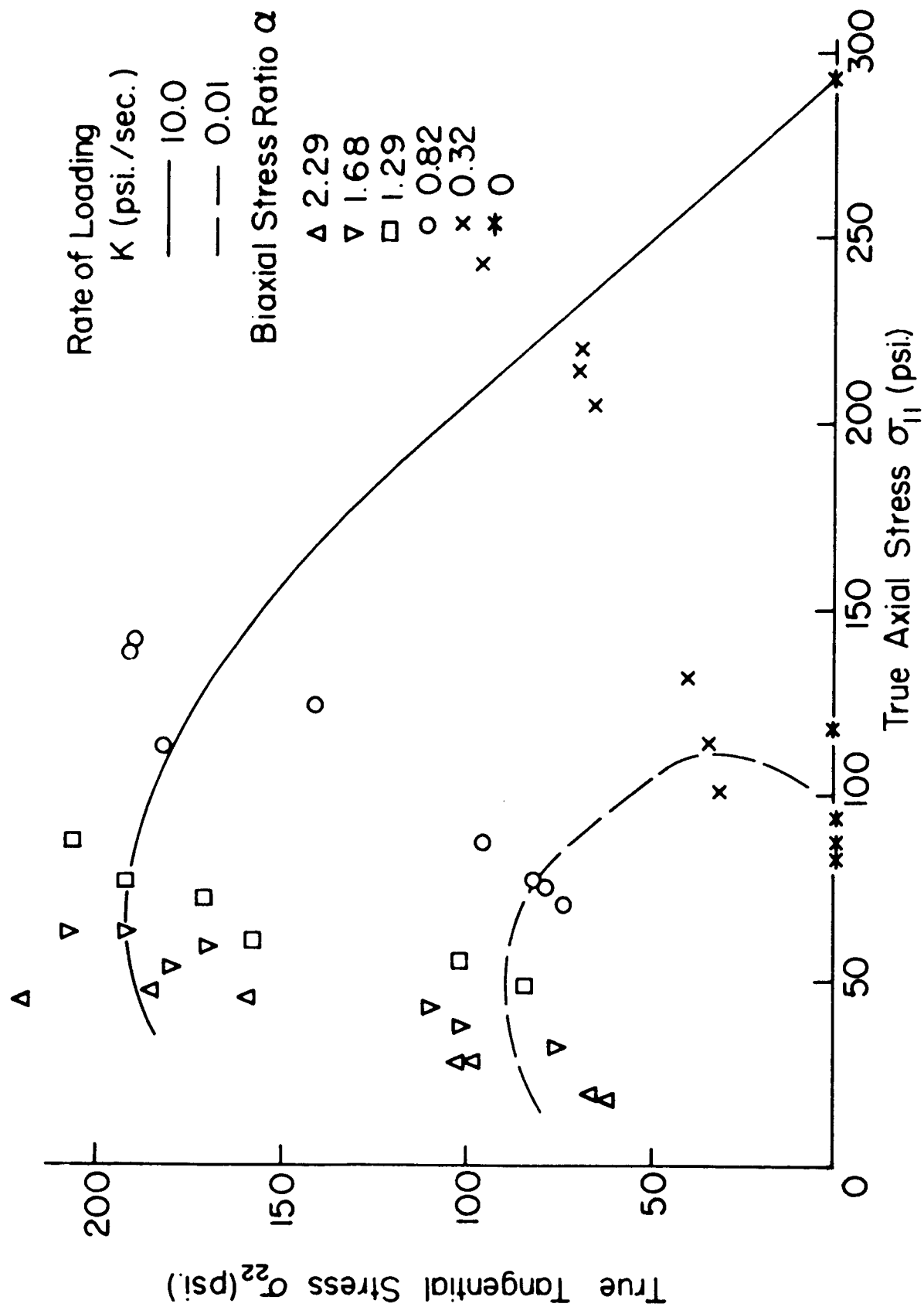
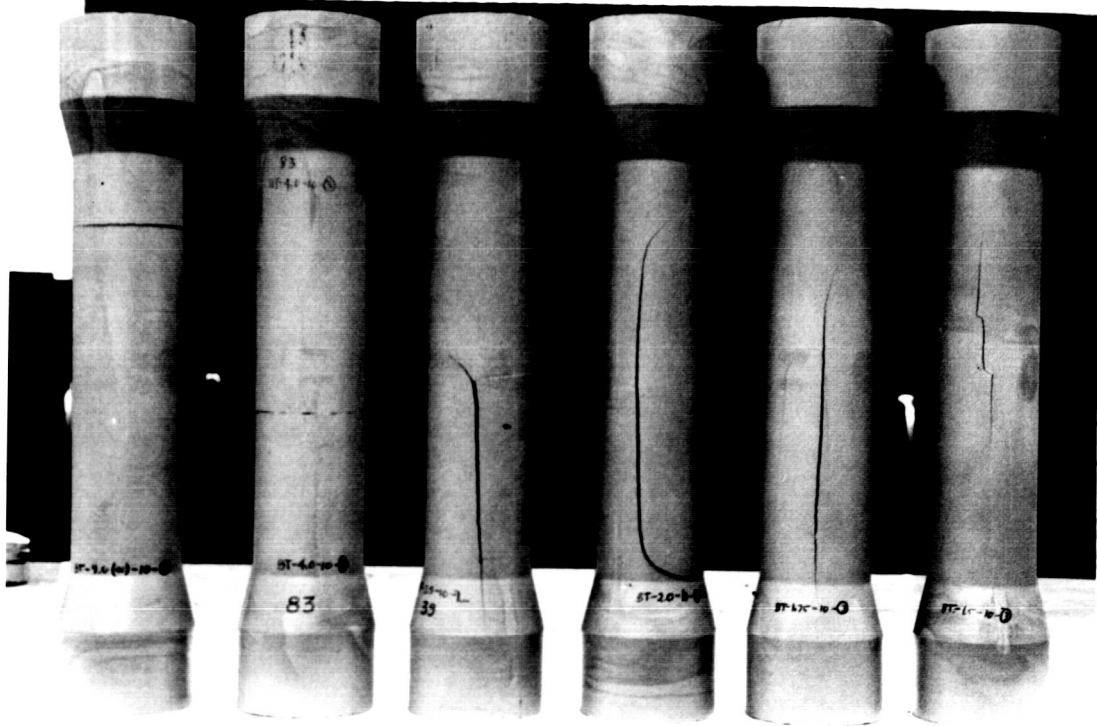
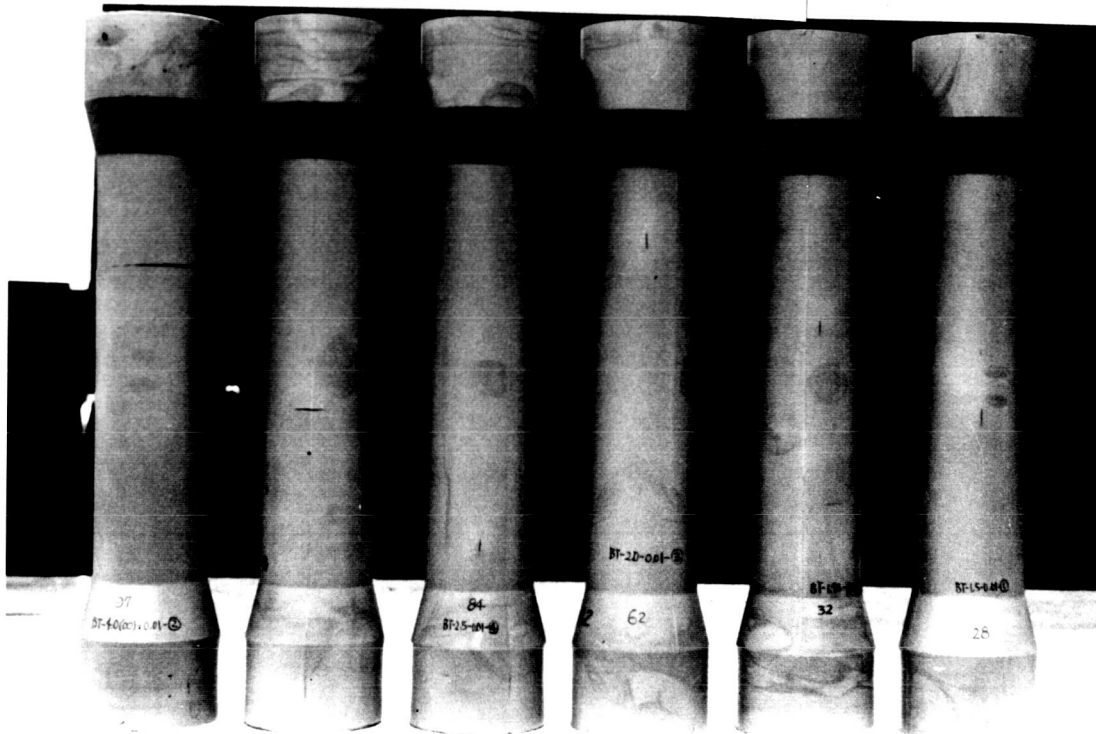


FIG. 16 FRACTURE CURVES FOR THE INERT COMPOSITE PROPELLENT



Rate of Loading  $k = 10 \text{ psi/sec}$



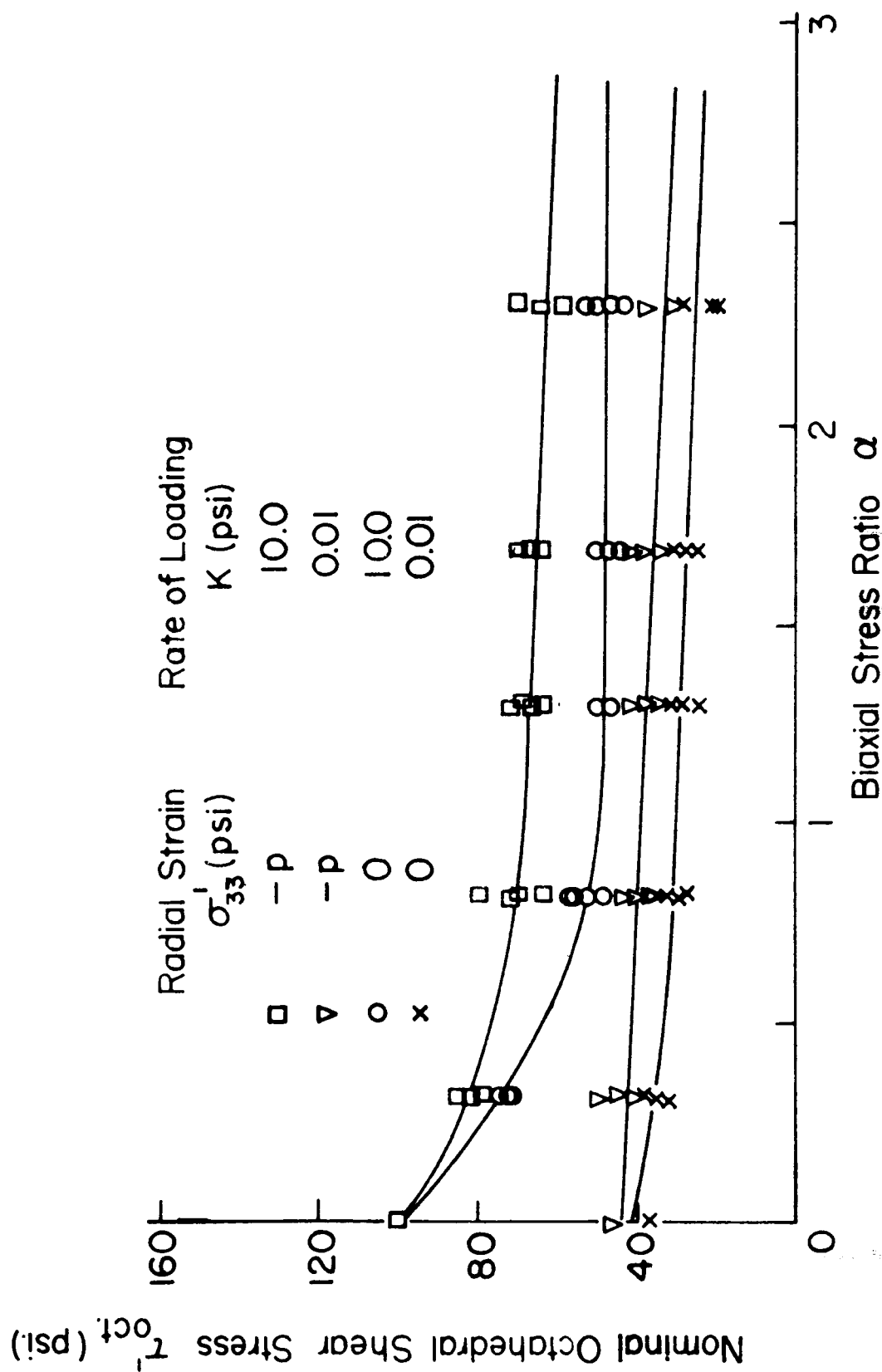


FIG. 18 VARIATION OF NOMINAL OCTAHEDRAL SHEAR STRESS WITH BIAxIAL STRESS RATIO

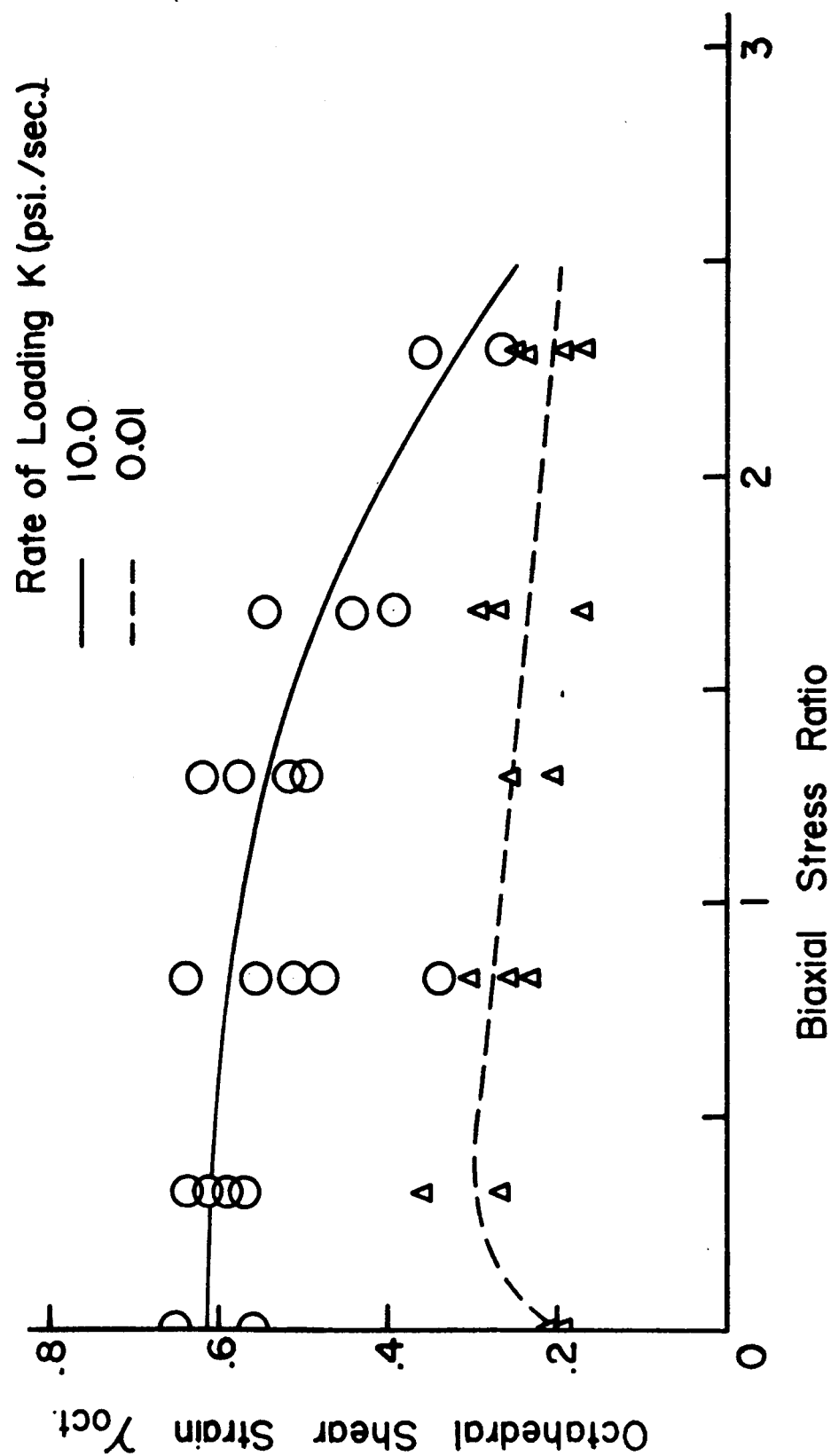


FIG. 19 VARIATION OF OCTAHEDRAL SHEAR STRAIN WITH BIAxIAL STRESS RATIO

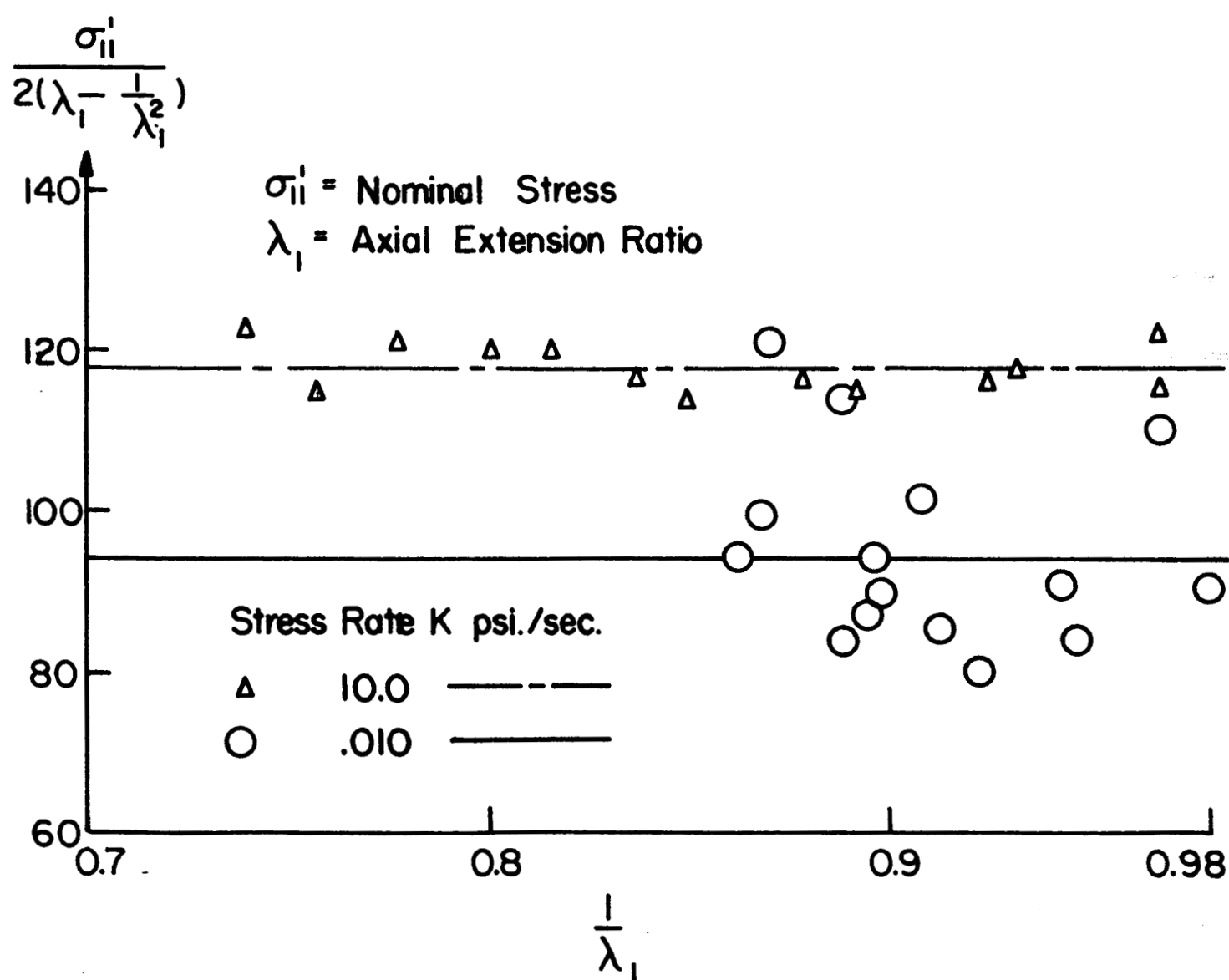


FIG. 20 PLOT OF  $\sigma'_{11} / 2(\lambda_1 - \frac{1}{\lambda_1^2})$  AGAINST  $\frac{1}{\lambda_1}$  FROM SIMPLE TENSION EXPERIMENTS

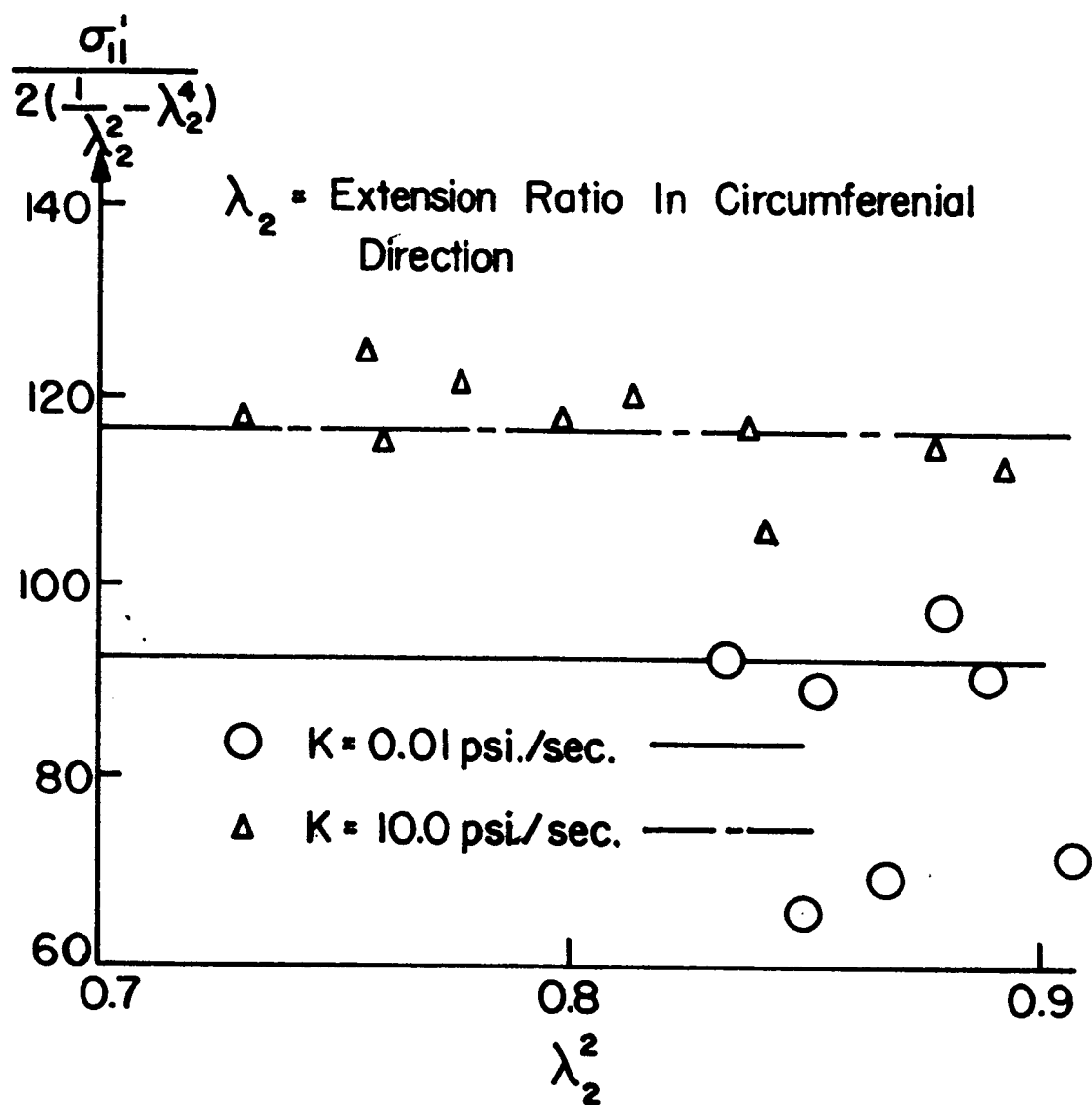


FIG. 21 PLOT OF  $\frac{\sigma_{11}'}{2(\frac{1}{\lambda_2^2} - \lambda_2^4)}$  AGAINST  $\lambda_2^2$  FROM SIMPLE TENSION EXPERIMENTS

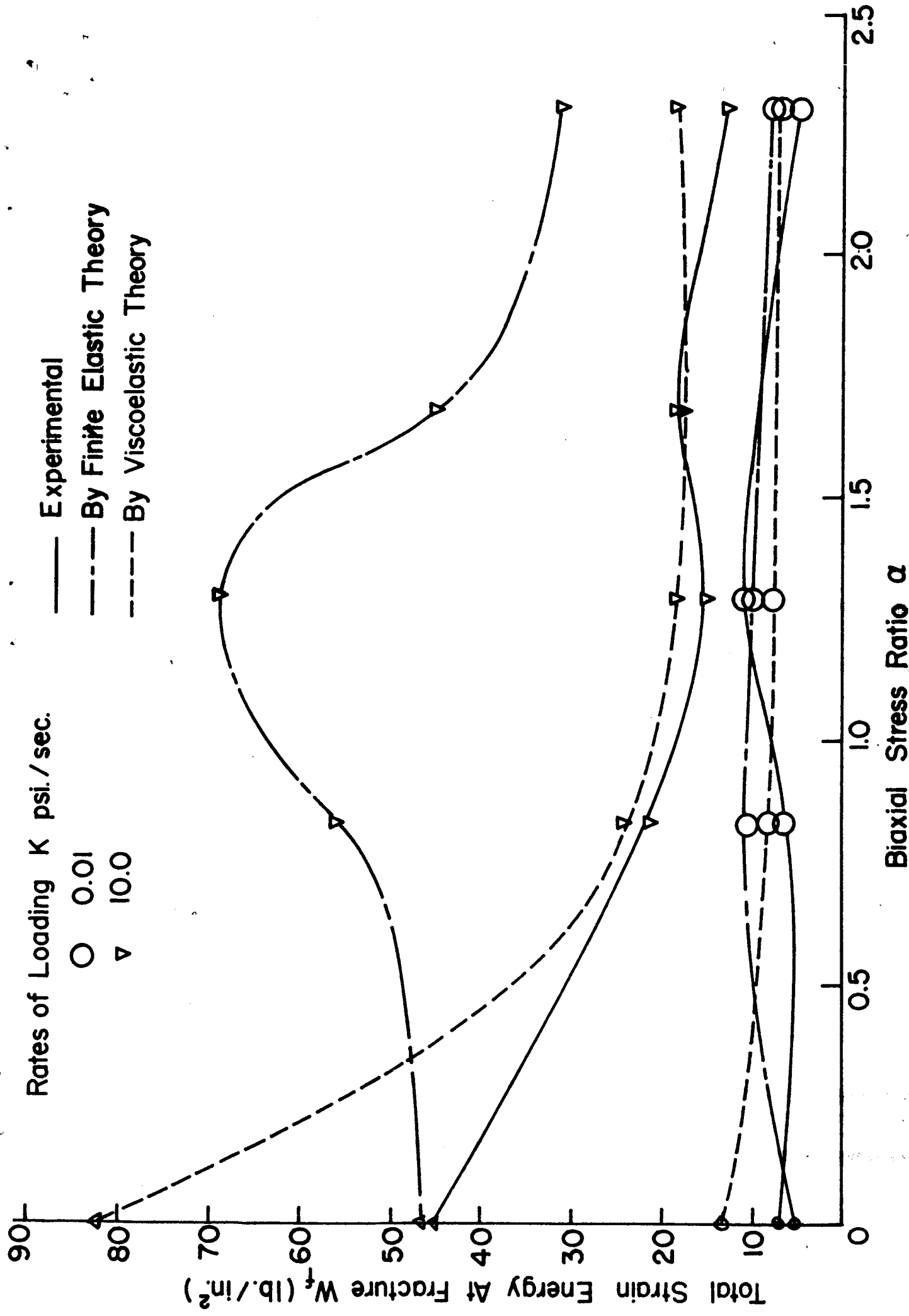


FIG. 22 VARIATION OF TOTAL STRAIN ENERGY AT FRACTURE WITH BIAxIAL STRESS RATIO FOR THE INERT COMPOSITE PROPELLENT